NASA Technical Memorandum 108808

A Direct Application of the Non-Linear Inverse Transformation Flight Control System Design on a STOVL Aircraft

W. W. Chung, W. E. McNeill, and M. W. Stortz
Ames Research Center, Moffett Field, California

May 1993

National Aeronautics and
Space Administration

Ames Research Center
Moffett Field, California 94035-1000

Nomenclature

AX_{CMD}	generalized acceleration command, stability axis, ft/sec^2
AYP	lateral acceleration, pilot station, body axis, ft/sec^2
AZ_{CMD}	generalized acceleration command, stability axis, ft/sec^2
d_{x2d}	2-DCD nozzle axial moment arm, ft
d_{xej}	ejector axial moment arm, ft
d_{xvn}	ventral nozzle axial moment arm, ft
d_{z2d}	2-DCD nozzle vertical moment arm, ft
d_{zvn}	ventral nozzle vertical moment arm, ft
$D_{(\Delta D/T)T}$	aerodynamic drag due to thrust, lb
$D_{(\Delta L/T)T}$	aerodynamic lift due to thrust, lb
D_{2DZ}	2-DCD nozzle thrust vertical moment arm, ft
D_{AERO}	drag due to aerodynamics, lb
D_{VNZ}	ventral thrust vertical moment arm, ft
L_{AERO}	lift due to aerodynamics, lb
m	mass of E-7D, slug
$M_{(\Delta/T)T}$	pitching moment due to thrust induced aerodynamics, ft-lb
M_{AERO}	pitching moment due to aerodynamics, ft-lb
M_{GYRO}	pitching moment due to engine's gyscopic effect, ft-lb
M_{INLET}	pitching moment due to inlet forces, ft-lb
p	roll rate, body axis, rad/sec
p_{cmd}	roll rate command, deg/sec
$\bar{q}$	dynamic pressure, lb/ft^2
q	pitch rate, body axis, rad/sec
$\dot{q}$	pitch angular acceleration, body axis, rad/sec^2
r	yaw rate, body axis, rad/sec
r_{cmd}	yaw rate command, deg/sec
V_{GX}	longitudinal ground velocity, ft/sec
V_{GY}	lateral ground velocity, ft/sec
W	weight of E-7D, lb
X_{2DC}	2-DCD nozzle thrust command, axial component, lb
X_{INLET}	inlet induced force, axial component, lb
X_{VNC}	ventral nozzle thrust command, axial component, lb
Z_{2DC}	2-DCD nozzle thrust command, vertical component, lb
Z_{INLET}	inlet induced force, vertical component, lb
Z_{VNC}	ventral nozzle thrust command, vertical component, lb

Symbols

α_c	commanded angle of attack, rad
β	sideslip angle, rad
β_{cmd}	sideslip angle command, degree
δ_{lat}	lateral side arm stick, lb
δ_{lon}	longitudinal side arm stick, lb
δ_{ped}	pedal, lb
δ_{th}	throttle position, in.
δ_{amb}	ambient air density ratio, n.d.
ϕ	roll attitude, deg
γ	flight path angle, rad
γ_c	commanded flight path angle, rad
θ	pitch attitude, deg
θ_{2DC}	2-DCD nozzle deflection command, deg
θ_{VNC}	ventral nozzle deflection command, deg
ΔD_{PROP}	required longitudinal propulsion thrust, stability axis, lb
ΔL_{PROP}	required vertical propulsion thrust, stability axis, lb
ΔM	demanded propulsive pitching moment, ft-lb
ΔX	demanded axial propulsive thrust, body axis, lb
ΔZ	demanded vertical propulsive thrust, body axis, lb

Direct Application of the Non-Linear Inverse Transformation Flight Control System Design on a STOVL Aircraft

W. W. CHUNG, W. E. MCNEILL, AND M. W. STORTZ

Ames Research Center

Summary

The non-linear inverse transformation flight control system design method is applied to the Lockheed Ft. Worth Company's E-7D short takeoff and vertical land (STOVL) supersonic fighter/attack aircraft design with a modified General Electric F110 engine which has augmented propulsive lift capability. The system is fully augmented to provide flight path control and velocity control, and rate command attitude hold for angular axes during the transition and hover operations. In cruise mode, the flight control system is configured to provide direct thrust command, rate command attitude hold for pitch and roll axes, and sideslip command with turn coordination. A control selector based on the non-linear inverse transformation method is designed specifically to be compatible with the propulsion system's physical configuration which has a 2 dimensional convergent-divergent aft nozzle, a vectorable ventral nozzle and a thrust augmented ejector. The non-linear inverse transformation is used to determine the propulsive forces and nozzle deflections, which in combination with the aerodynamic forces and moments (including propulsive induced contributions), and gravitational force, are required to achieve the longitudinal and vertical acceleration commands. The longitudinal control axes are fully decoupled within the propulsion system's performance envelope.

A piloted motion-base flight simulation was conducted on the Vertical Motion Simulator at NASA Ames Research Center to examine the handling qualities of this design. Based on results of the simulation, refinements to the control system have been made and will also be covered in the report.

Introduction

The non-linear inverse transformation flight control system design method has been successfully applied on two short takeoff and vertical landing (STOVL) aircraft (refs. 1 and 2). Level 1 flying qualities for approach and landing, including shipboard landing under adverse wind conditions, were achieved during these motion based flight simulations. The generality of this design method simplifies the control design process by decoupling the longitudinal control axes and by solving the STOVL control redundancy through the inverse transformation of the force and moment equations. The regulator of the flight control system is an implicit model following design which provides desirable closed-loop performance in all axes. The purpose of this experiment is to evaluate the applicability of this design procedure to the E-7D STOVL aircraft with a component level propulsion system model, and to examine the handling qualities of the closed-loop system for approach and landing flight operations.

This report describes the basic aircraft with augmented lift capable propulsion system, the augmented flight control system, the flight simulation experiment, and the refinement of the final control system design.

Aircraft Description

The Lockheed Ft. Worth Company's (LFWC) E-7D is a single-seat, single-engine STOVL supersonic fighter/attack aircraft. Both E-7D's airframe design and GE's F110 turbofan engine derivative have undergone extensive research and development through the STOVL supersonic fighter/attack aircraft program which was sponsored jointly by the governments of the United States and the United Kingdom, and a program sponsored by NASA Lewis (LeRC) employing Design Methods for Integrated Control Systems (DMICS). The E-7D is an enhanced version of the earlier E-7A configuration which was developed under contract to NASA Ames Research Center (ARC) (ref. 3). The major difference between the two versions is the propulsion system's configuration. The E-7A employed split flow, where fan air flow was ducted to the ejectors and to the aft nozzle and core flow was routed to the vectorable ventral nozzle, while the E-7D utilized mixed fan and core flow to all three thrust nozzles.

Airframe

The E-7D airframe is based on the LFWC's F-16-fuselage (fig. 1). The aircraft has a tailless delta wing configuration

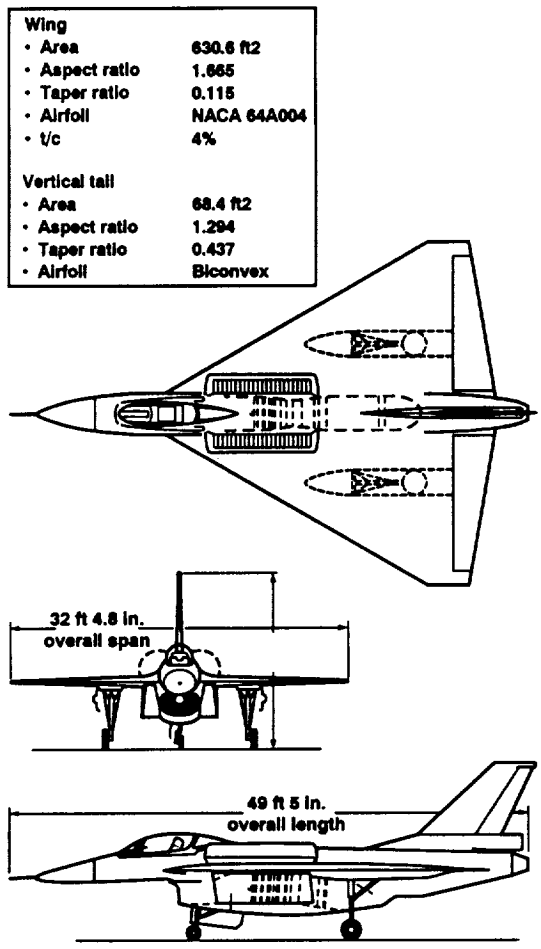

Figure 1. Three views of Lockheed Ft. Worth Company (LFWC) E-7D STOVL design.

with a sweep angle of 60° and an aspect ratio of 1.67. The aerodynamic control surfaces include elevons and a rudder. The elevons, which have a range of deflection of ±30°, provide both pitch and roll control power. The pitch control power is generated by deflecting the left and right elevons symmetrically, and roll control power is generated by deflecting elevons differentially. The rudder has a deflection range of ±20°.

The aerodynamic data for this experiment are based on extensive wind tunnel tests and theoretical estimates. The data base includes power induced aerodynamics and ground effects.

Propulsion System

The propulsion system of this aircraft is a GE Aircraft Engines (GEAE) F110 turbofan engine derivative (fig. 2). This engine has a high pressure system which consists of 9-stage high pressure compressor, an annular combustor,

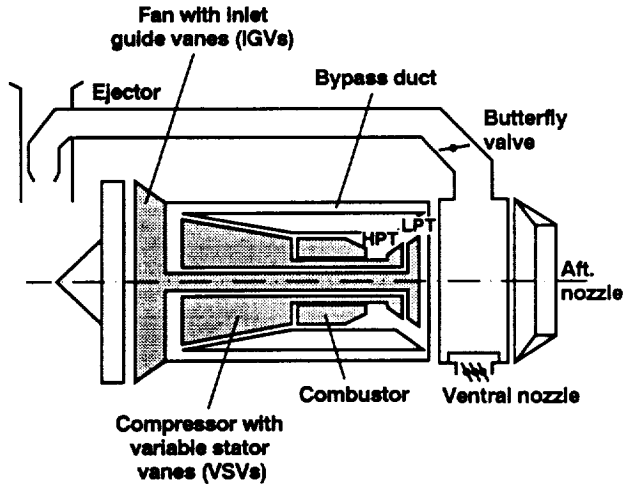

Figure 2. General Electric Aircraft Engines (GEAE) F110/STOVL engine.

and a single stage high pressure turbine, and a low pressure system which consists of a 3-stage fan driven by a 2-stage low pressure turbine (ref. 4). The overall pressure ratio is about 30 to 1. The maximum gross thrust is about 19,000 lb.

The hot air from the core, after mixing with the cold air from the bypass duct, is directed to a 2-dimensional convergent-divergent (2-DCD) nozzle, a vectoring ventral nozzle, and through a butterfly valve to two sets of ejector nozzles mounted along the wing roots. During cruise flight, both ventral and ejector doors are closed and exhaust flow exits at the 2-DCD nozzle. For transition and hovering flight, the ejector and ventral doors are opened to generate direct propulsive lift. The ejector flow is modulated through the butterfly valve and the ventral nozzle area is modulated using louvers. The 2-DCD nozzle can be deflected between ±20°. The ventral nozzle can be vectored from 50° to 110° with respect to the waterline, i.e., 40° aft and 20° forward of the vertical axis. The 2-DCD nozzle is closed completely during the hover operations. With the upper ejector doors opened, the lift produced by the ejectors is further augmented through mixing the exhaust with the airflow entrained through the top doors. There are five Reaction Control System (RCS) exhaust nozzles located in the nose and wing tips. The RCS can draw a maximum of 7% of the engine compressor discharge flow. The nozzle areas are modulated via individual actuators. The RCS provides the roll, pitch and yaw control power during transition and hover flight.

A component level model (CLM) of this engine was developed by GEAE under a NASA contract with LeRC as a part of a study to validate the DMICS methodology. The model is assembled with each major component of

the engine, which includes inlet, fan, high pressure compressor, bypass duct, main burner, high pressure turbine, lower pressure turbine, exit flow mixing, nozzle thrust calculation, and a propulsion control system with a multivariable regulator and a rapid thrust modulation (RTM) control. The performance of the engine is designed to meet both small and large magnitude specifications generated by LFWC under the same contract with LeRC. In general, the propulsion system has a bandwidth of 10 rad/sec.

Flight Control System

The flight control system consists of three major components as shown in figure 3. They are command generator, regulator and control selector. The command generator shapes the pilot inputs and generates control commands based on the control mode and respective control augmentation. The regulator employs an implicit model following state rate feedback design to generate a set of generalized control commands to provide stability and control augmentation. The control selector then converts the generalized acceleration control commands to physical aerodynamic control effector position commands and individual nozzle thrust and angle deflection commands.

Command Generator

The command generator selects the control inceptors from the cockpit, shapes the pilot control inputs, and generates control commands corresponding to the flight control mode. Three flight modes are used in this design which are cruise, transition and hover. The primary control inceptors are an F-16 limited displacement 2-axis side arm force controller, a linear throttle control with a thumb wheel, and limited displacement force pedals.

In the cruise mode, the throttle commands total thrust. The longitudinal and lateral side arm controller generates pitch and roll rate command respectively. A 4-position trim switch, on top of the 2-axis side arm controller, provides pitch and roll attitude trim. The rudder pedals are used for sideslip command.

After the flight path command augmentation is engaged during the transition mode, all the control inceptor functions remain the same as for the cruise mode except the throttle. The throttle is augmented to provide flight path command and the thumb wheel, located on the throttle grip, is added to control the acceleration along the flight path with velocity hold.

In the hover mode, the 2-axis side arm controller is switched to control longitudinal and lateral ground velocity. The throttle commands vertical velocity and the pedal commands yaw rate. The roll trim function of the 4-position switch is deactivated. The pitch trim switch is still functional. A separate 4-position switch, also located on the side arm controller, is used for ground velocity trim. The thumb wheel on the throttle grip is disconnected in this mode. All the control modes and control inceptor configurations are shown in figure 4. The control sensitivities for all control inceptors are shown in figures 5–9.

Regulator

The regulator design is adapted directly from a Mixed Flow Vectored Thrust (MFVT) STOVL experiment (ref. 2). The structure of the overall control system remains the same. Only the physical system limits and control sensitivities are modified to conform with the system characteristics of the E-7D. It applies a state-rate feedback-implicit model following the design to all control axes except the yaw control axis in cruise and transition. The characteristics of the flight modes and corresponding implicit models are shown in table 1. The output of the regulator is a set of generalized acceleration control commands that are fed into the control selector.

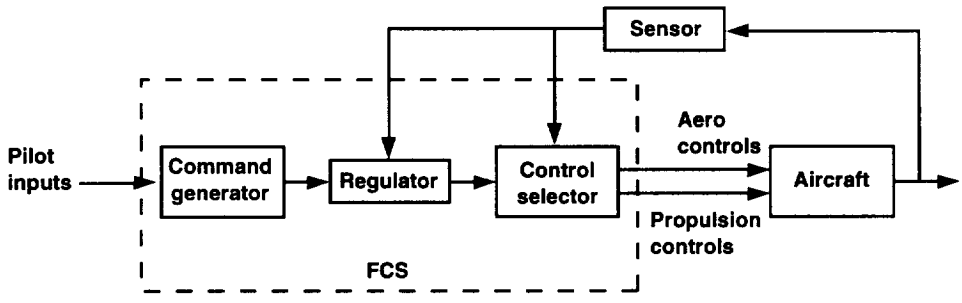

Figure 3. Flight control system (FCS) structure.

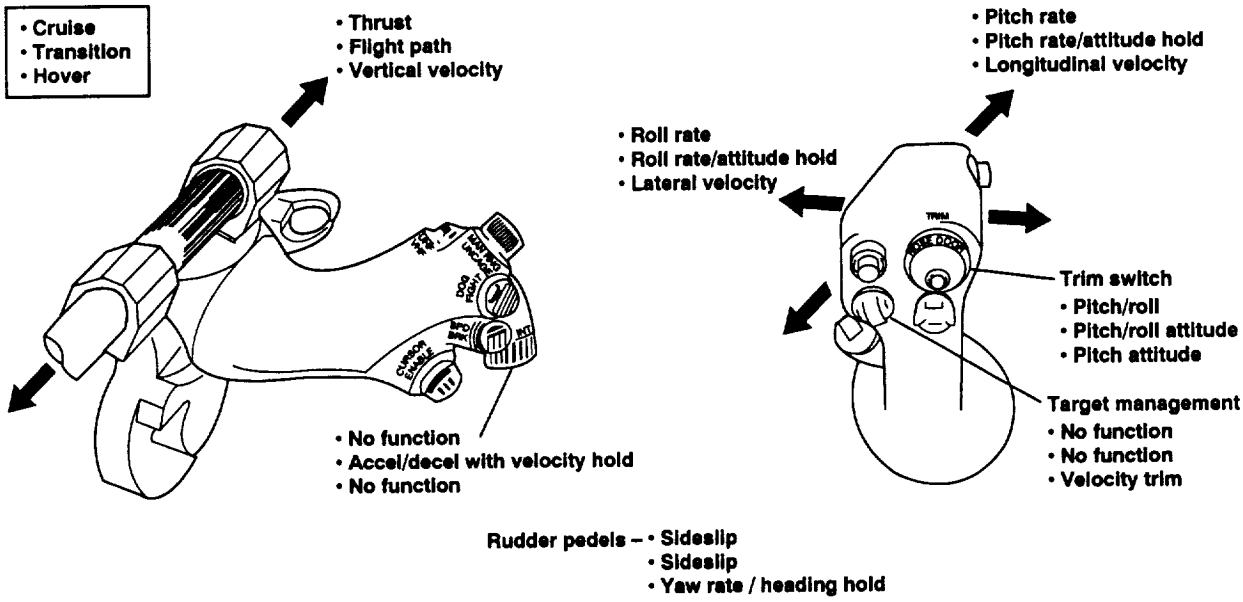

Figure 4. Control modes and control inceptor configurations.

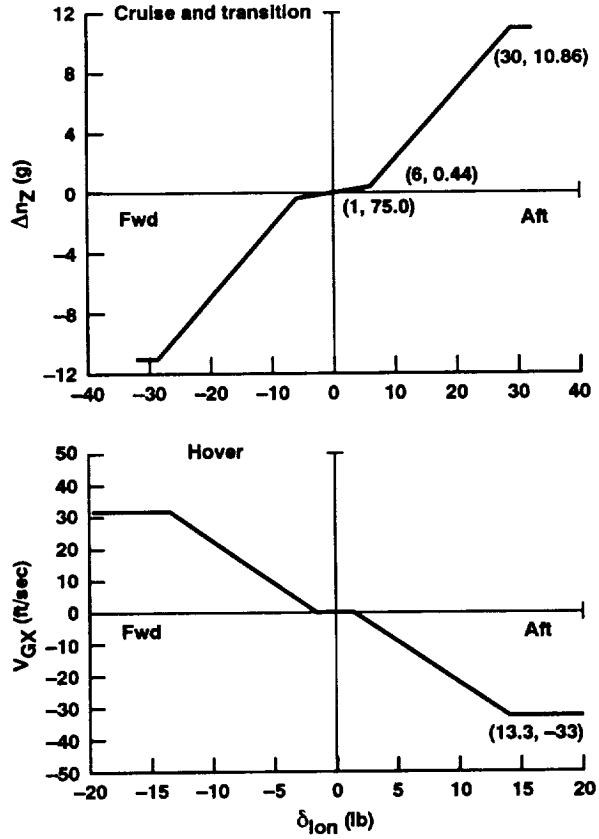

Figure 5. Longitudinal side arm controller command schedule.

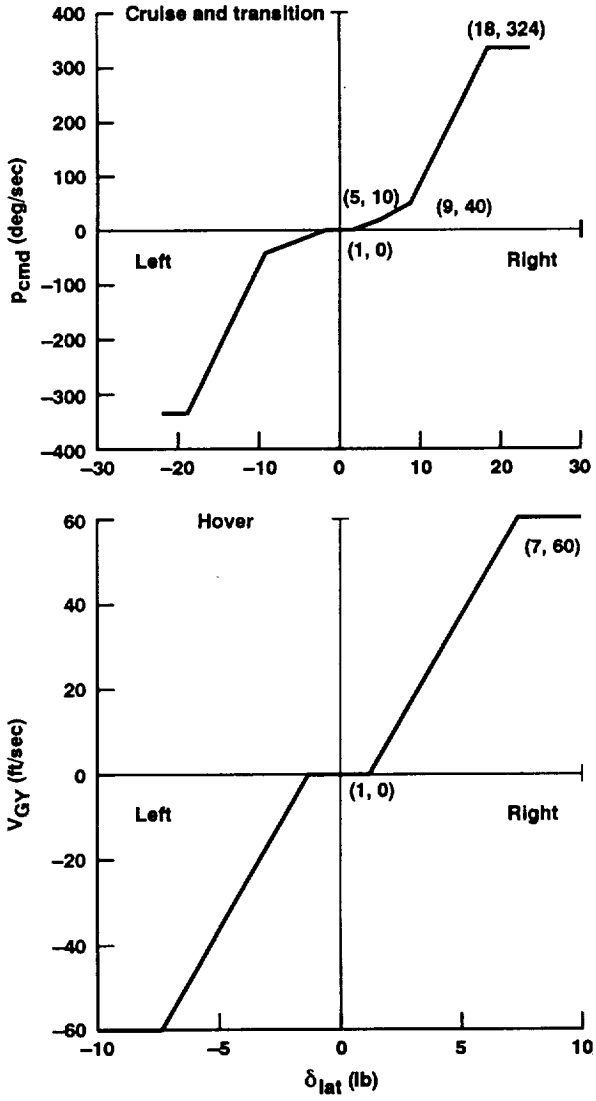

Figure 6. Lateral side arm controller command schedule.

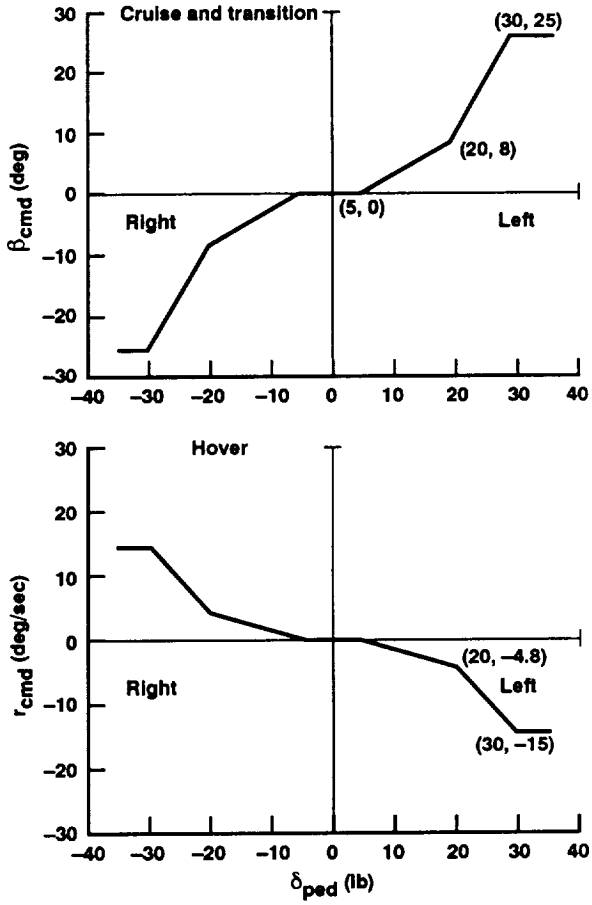

Figure 7. Pedal command schedule.

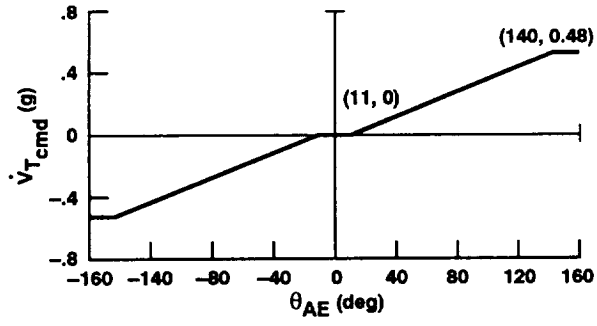

Figure 8. Throttle thumb-wheel command schedule.

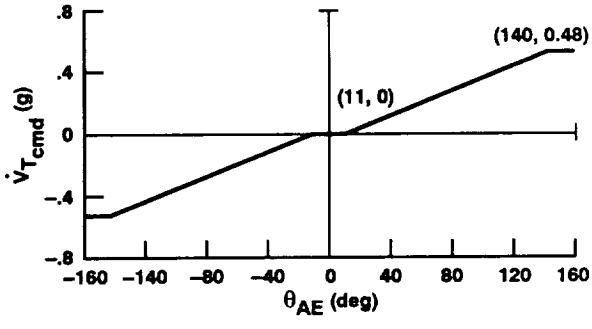

Figure 9. Throttle command schedule.

Table 1. Implicit model following control mode dynamics

Control axis	Transition	Hover	Effector
Pitch	$\frac{\dot{\theta}}{\dot{\theta}_c} = \frac{4}{(s+2)^2}$	$\frac{\dot{\theta}}{\dot{\theta}_c} = \frac{4}{(s+2)^2}$	±30° Symmetrical elevons 0–1,300 lb RCS thrust ±20° cruise nozzle
Roll	$\frac{\dot{\phi}}{\dot{\phi}_c} = \frac{9}{s^2+7s+9}$	$\frac{\dot{\phi}}{\dot{\phi}_c} = \frac{9}{s^2+7s+9}$	±30° Differential elevons 0–1,300 lb RCS thrust
Yaw	$\frac{\Delta\beta}{\Delta\phi} \le 0.2$	$\frac{\dot{\psi}}{\dot{\psi}_c} = \frac{4}{s+4}$	±30° Rudder 0–1,300 lb RCS thrust
Vertical	$\frac{\gamma}{\gamma_c} = \frac{1}{s^2+1.4s+1}$	$\frac{\dot{h}}{\dot{h}_c} = \frac{1}{s^2+1.4s+1}$	1,000–19,000 lb thrust
Longitudinal	$\frac{V_x}{V_{xc}} = \frac{0.5(s+0.7)(s+2.86)}{s(s^2+1.8s+1.0)}$	$\frac{V_x}{V_{xc}} = \frac{0.35(s+2.86)}{s^2+1.8s+1.0}$	0–110° θ_n
Lateral	Same as yaw	$\frac{V_y}{V_{yc}} = \frac{1.75^3}{(s+1.75)^3}$	

For the angular control and stabilization, a rate command attitude hold response is provided for both pitch and roll controls in cruise and transition modes. The pitch control block diagram is shown in figure 10. The feedback of the first order lag, and pitch attitude, rate and acceleration constitute the implicit state-rate feedback model following system which guarantees the control stability and minimum steady state error. The control sensitivity gain, K_{300}, is scaled as a function of dynamic pressure to maintain a constant forward loop control sensitivity throughout the flight envelope. It is defined as follows:

$$K_{300} = \frac{K_{300hover}}{1 + K_{\ddot{\theta}}\bar{q}}$$

where $K_{\ddot{\theta}}$ is calculated from the slope of the pitch control power curve of the E-7D (fig. 11) dividing by the product of $K_{300hover}$ and the maximum elevator deflection (symmetrical elevons). The control power curve is the maximum combined pitch angular acceleration authority of the aerodynamic control effector, i.e., elevons, and RCS jets. $K_{300hover}$ is sized from the maximum pitch control authority of the MFVT STOVL experiment in hover. It is defined as follows:

$$\ddot{\theta}_{max} \cdot K_{300hover}\Big|_{E7} = \ddot{\theta}_{max} \cdot K_{300hover}\Big|_{MFVT}$$

The roll control design in the cruise and transition modes is similar to that for the pitch axis (fig. 12). The loop gain K_3 is scaled in the same manner as K_{300} to maintain constant roll axis control sensitivity.

$$K_3 = \frac{K_{3hover}}{1 + K_{\ddot{\phi}}\bar{q}}$$

where $K_{\ddot{\phi}}$ is the slope of the roll control power curve of the E7-D (fig. 13) dividing by the product of K_{3hover} and the maximum aileron deflection (differential elevons), and K_{3hover} is sized from the maximum roll control authority between the two models in the same manner as the pitch axis. In hover mode, since there is no direct lateral thrust generator in this aircraft, the lateral velocity control is achieved by banking the aircraft to generate horizontal thrust component. The lateral velocity command closes the loop with lateral ground velocity and roll attitude.

The yaw control provides sideslip command with turn coordination during the cruise and transition modes, and yaw rate command/heading hold in hover mode. The state-rate feedback model following design is used in the hover mode for precise heading control. The yaw control and stabilization block diagram is shown in figure 14.

The flight path command augmentation includes a longitudinal velocity control loop and a vertical velocity control loop. Both loops apply the implicit model following design for precise velocity control. The block diagrams of these two regulator loops are shown in figures 15 and 16. Since the bandwidth of the GE F110 derivative propulsion system is the same as that of the previous MFVT

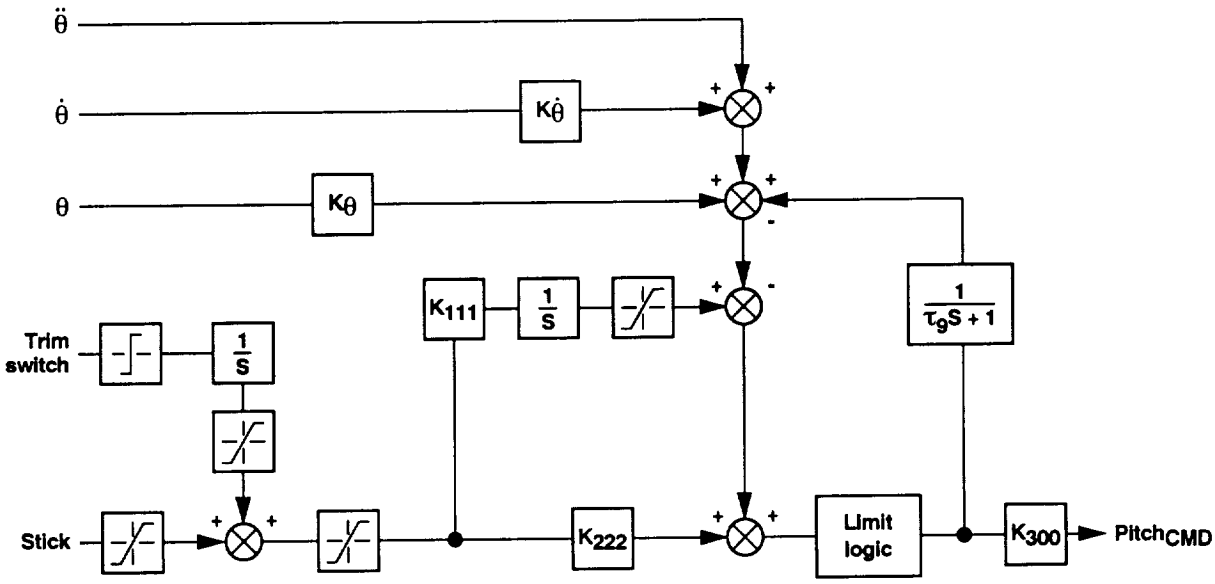

Figure 10. Pitch stabilization and command augmentation system.

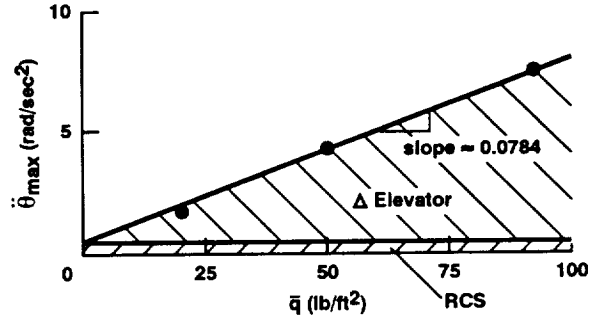

Figure 11. Combined maximum pitch control power.

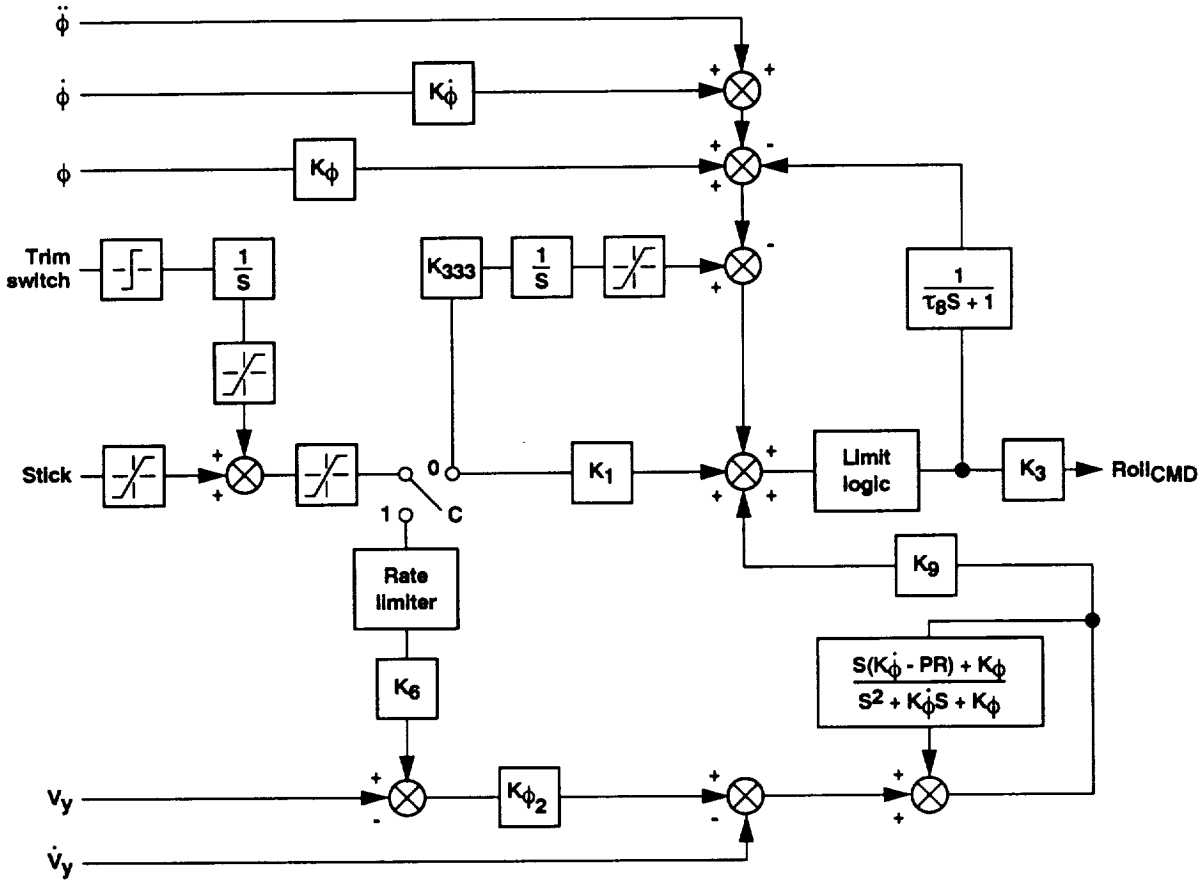

Figure 12. Roll and lateral velocity stabilization and command augmentation system.

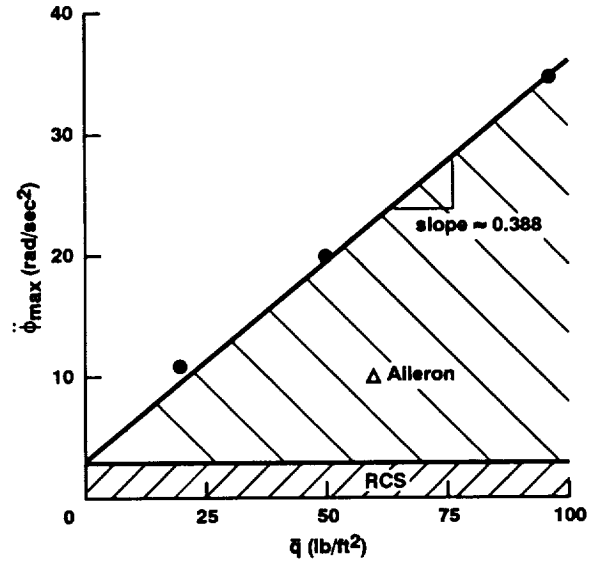

Figure 13. Combined maximum roll control power.

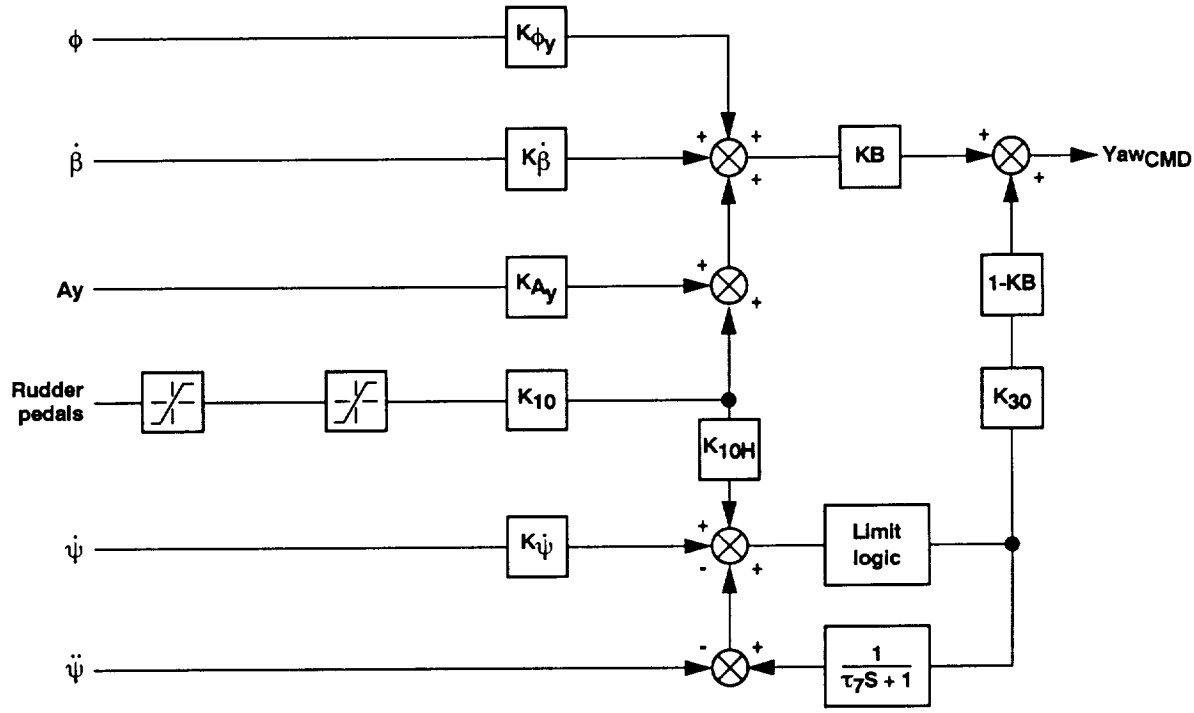

Figure 14. Yaw stabilization and command augmentation system.

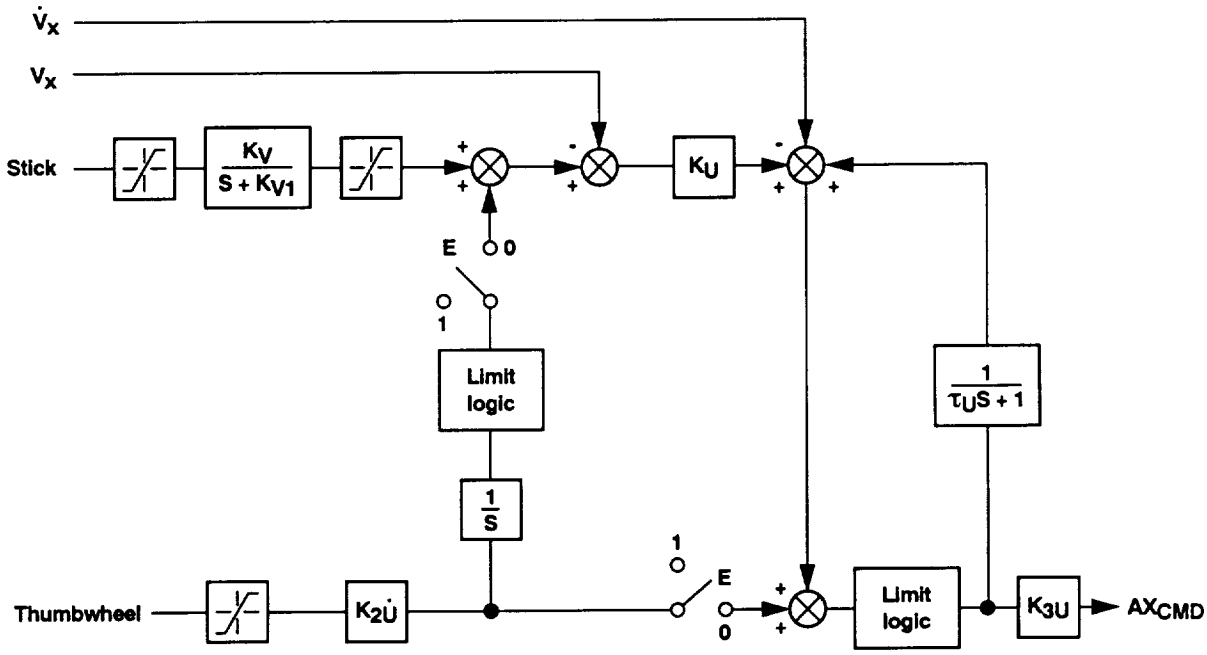

Figure 15. Longitudinal velocity stabilization and command augmentation system.

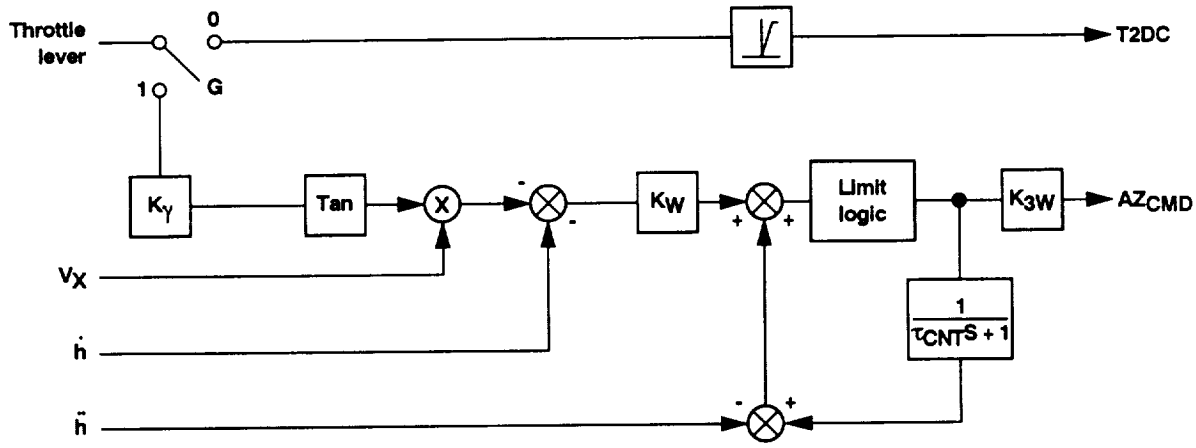

Figure 16. Vertical velocity stabilization and command augmentation system.

experiment's linear engine (10 rad/sec), the loop gains K_{3U} and K_{3W} are kept the same as the MFVT.

The first estimate of control loop gains were all sized from the MFVT experiment. Subsequent modifications were required to fine tune each individual control axis response. The final control loop gains are listed in table 2.

Control Selector

The control selector converts the generalized control commands to physical actuator commands and thrust commands. All of the E-7D's physical control actuators and thrust command stations are shown in figure 17. Aerodynamic control surfaces, such as elevons and rudder, and the RCS, which is part of the propulsion system, are partitioned to be angular acceleration control effectors. Thrust magnitude and deflection from the individual nozzles are used exclusively for longitudinal and vertical acceleration controls, and for maintaining pitch trim.

The generalized pitch acceleration command is mixed with the generalized roll acceleration command to generate left and right elevon actuator commands (fig. 18) and RCS area commands for the nose RCS and the up and down wingtip RCS. The pitch acceleration command leads to symmetrical left-wing and right-wing elevon deflections. It also leads to the nose RCS area actuator command and symmetrical up or down RCS area actuator commands at the wingtips. The RCS actuator command generator is shown in figure 19. The roll acceleration command leads to differential elevons deflections and asymmetrical up or down RCS area actuator commands at the wingtips. The generalized yaw acceleration control command is converted to rudder deflection and yaw RCS area actuator commands at the wingtips.

The thrust management system (TMS) applies non-linear inverse transformation to fully decouple the longitudinal, vertical, and pitch control axes to achieve the generalized axial and vertical acceleration control commands. A general structure of the TMS is shown in figure 20. The acceleration contributions from known aerodynamic lift and drag forces, thrust induced aerodynamic lift and drag forces, and gravitational components are first removed from the generalized acceleration control commands which are in the aircraft's stability axes.

$$\Delta D_{PROP} = -m\,AX_{CMD} - D_{AERO} - D_{(\Delta D/T)T} - W\sin\gamma_c$$

$$\Delta L_{PROP} = -m\,AZ_{CMD} - L_{AERO} - L_{(\Delta L/T)T} + W\cos\gamma_c$$

The required propulsive lift and drag forces, ΔD_{PROP} and ΔL_{PROP}, are then transformed to the aircraft body axes. The forces induced by the inlet are then removed to determine the net thrust demands along the fuselage axial and vertical axes.

$$\Delta X = -\Delta D_{PROP}\cos\alpha_c + \Delta L_{PROP}\sin\alpha_c - X_{INLET}$$

$$\Delta Z = -\Delta D_{PROP}\sin\alpha_c - \Delta L_{PROP}\cos\alpha_c - Z_{INLET}$$

The pitching moment generated by the propulsive thrusts has to maintain pitch trim with the pitching moment generated by the aerodynamics, gyroscopic effect from engine, thrust induced aerodynamic effects, and inlet forces. This leads to the third equation of motion to determine the required thrust magnitude and deflection of individual nozzles.

$$\Delta M = -(M_{AERO} - M_{GYRO} - M_{(\Delta/T)T} + M_{INLET})$$

The TMS distributes these axial and vertical thrust demands, based on the pitch trim authority of the propulsion system, to 2-DCD thrust command (T_{2DC}), 2-DCD nozzle angle deflection command (θ_{2DC}), ejector thrust command (T_{EJC}), ventral thrust command (T_{VNC}), and

Table 2. Control mode gains

Attitude control	
Pitch	**Roll**
K_{111} = 4.0 rad/sec/lb	K_1 = 1.0 rad/lb
K_{222} = 3.0 rad/lb	K_{333} = 6.0 rad/sec/lb
K_θ = 4.0 rad/rad	K_ϕ = 9.0 rad/rad
$K_{\dot\theta}$ = 4.0 sec	$K_{\dot\phi}$ = 6.0 sec
$K_{\ddot\theta}$ = 0.00638 r/s^2/lb/ft^2	$K_{\ddot\phi}$ = 0.00443 r/s^2/lb/ft^2
K_{300} = 18.54/(1 + $K_{\ddot\theta}\bar{q}$) deg/rad/s^2	K_3 = 5.17/(1 + $K_{\ddot\theta}\bar{q}$) deg/rad/s^2
τ_9 = 0.05 sec	τ_8 = 0.05 sec
Yaw – transition	**Yaw – hover**
K_{10} = 0.0698 rad/lb	K_{10H} = 0.0698 rad/lb
$K_{\dot\beta}$ = 3.0 sec	$K_{\dot\psi}$ = 4.0 sec
K_{Ay} = –1.25/$\bar{q}$ rad/ft/sec^2; $\bar{q}$ > 5 lb/ft^2	K_{30} = 40.0 deg/rad
= –0.25 $\bar{q}$ ≤ 5 lb/ft^2	K_B = 0.0(V_x < 20 knots); 1.0(V_x ≥ 20 knots)
$K_{\phi y}$ = –0.6 [$\bar{q}$/(1 + 0.035$\bar{q}$)]	τ_7 = 0.05 sec

Velocity control		
Longitudinal velocity	**Vertical velocity**	**Lateral velocity**
K_{2u} = 0.12	K_γ = 0.1163 rad/in.	K_6 = 1.0
K_{v1} = 20.0 sec^{-1}	K_W = 1 sec^{-1}	PR = 5.25
K_v = 14.0 ft/sec^2/lb	K_{3w} = 0.2	$K_{\phi 2}$ = 0.58 rad/ft/sec
K_u = 0.69 sec^{-1}	τ_{CNT} = 0.1 sec	K_9 = 0.285 rad/rad
K_{3u} = 0.4		
τ_u = 0.35 sec		

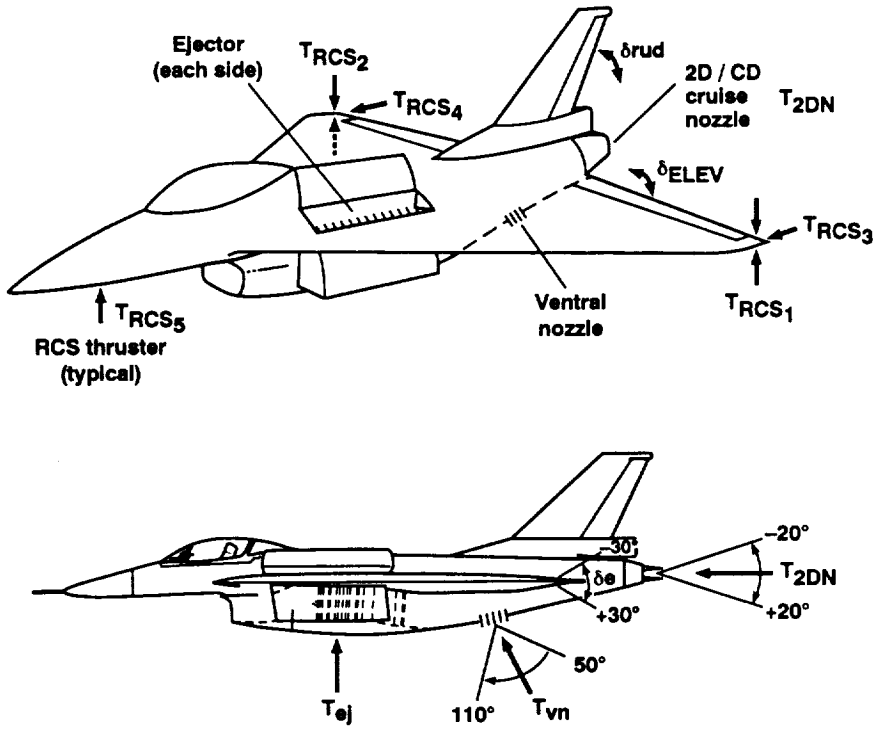

Figure 17. E-7D control effectors.

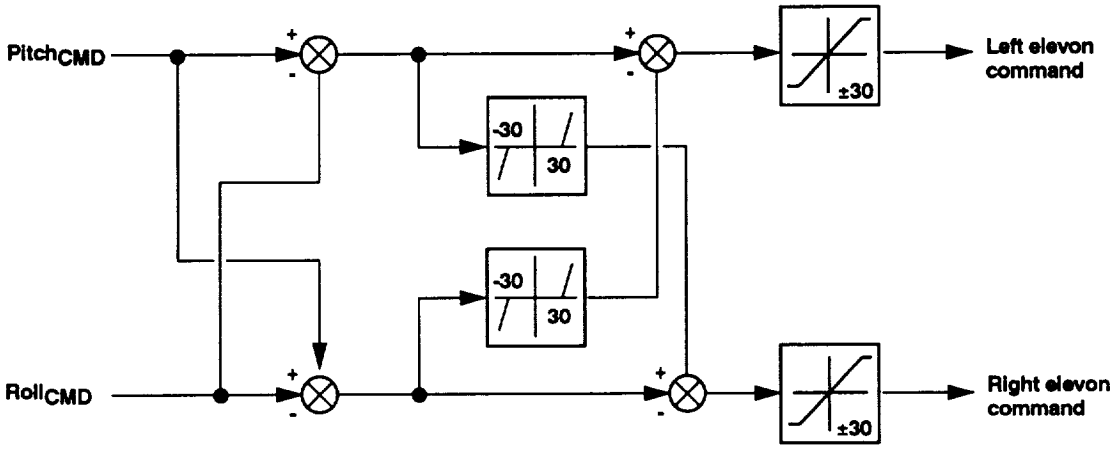

Figure 18. Elevons command generator.

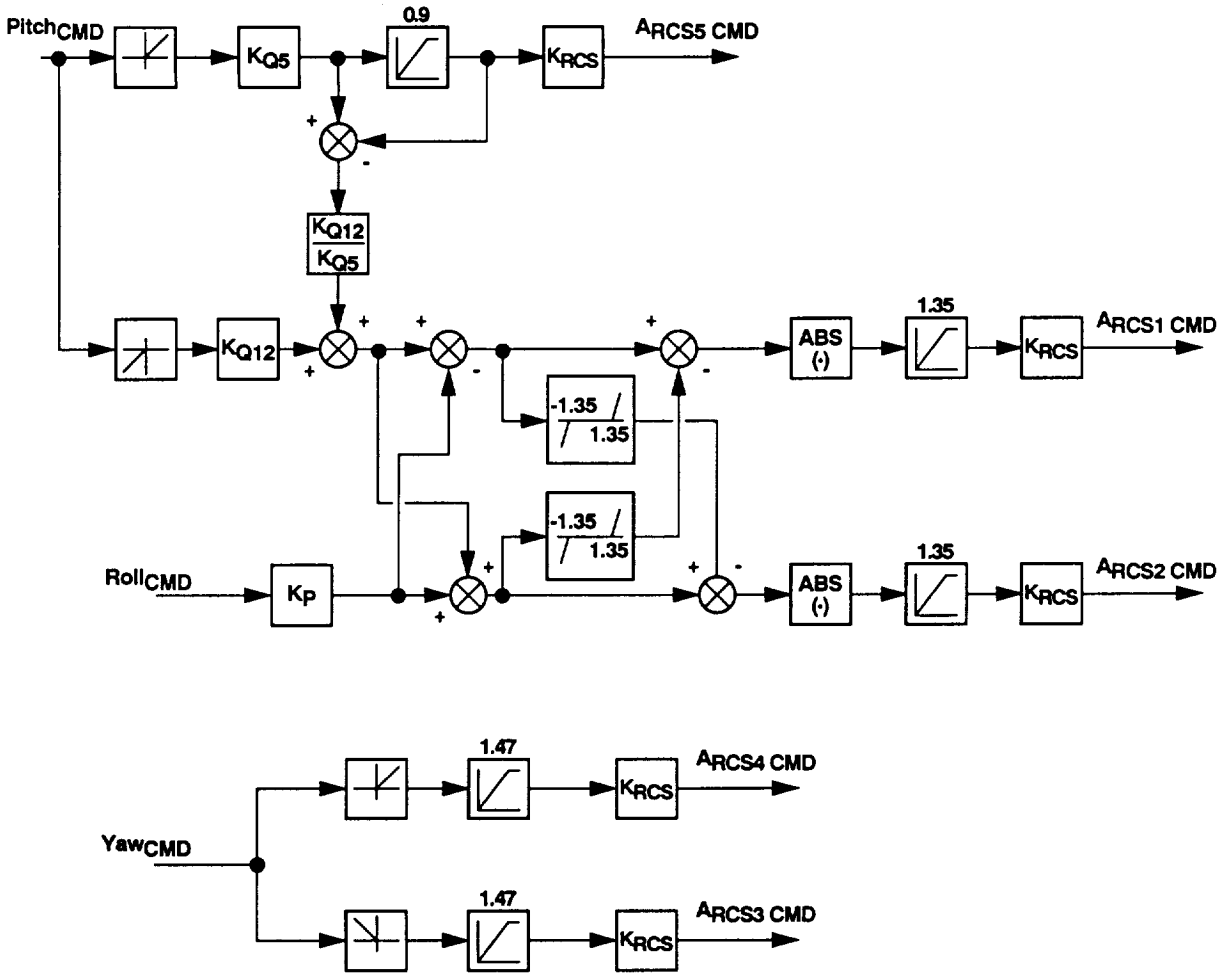

Figure 19. RCS command generator.

ventral nozzle angle deflection command (θ_{VNC}), based on the following phases of flight:

Wing borne– No vertical thrust is required from the propulsion system. 2-DCD nozzle angle is fixed at zero. Throttle control commands 2-DCD nozzle thrust directly. The total thrust command is governed by the following equation:

$$T_{2DC} = \delta_{th} \times f(T_{2DC}/\delta_{amb}, \delta_{th}) \times \delta_{amb}$$

where $f(T_{2DC}/\delta_{amb}, \delta_{th})$ is the thrust to throttle sensitivity. Pitch trim is provided by the aerodynamic control effectors.

High speed transition– Vertical thrust is required to meet the generalized vertical acceleration command. 2-DCD thrust and ejector thrust are used to provide axial and vertical thrust components, and 2-DCD nozzle deflection is used to maintain pitch trim. The 2-DCD nozzle thrust components, and ejector thrust are determined by solving the following three force and moment equations.

$$\Delta X = X_{2DC}$$

$$\Delta Z = Z_{2DC} - T_{EJC}$$

$$\Delta M = X_{2DC} \times |d_{z2d}| + Z_{2DC} \times |d_{x2d}| + T_{EJC} \times |d_{xej}|$$

which lead to:

$$\begin{bmatrix} X_{2DC} \\ Z_{2DC} \\ T_{EJC} \end{bmatrix} = \begin{bmatrix} 1 & 0 & 0 \\ 0 & 1 & 1 \\ |d_{z2d}| & |d_{x2d}| & |d_{xej}| \end{bmatrix}^{-1} \begin{bmatrix} \Delta X \\ \Delta Z \\ \Delta M \end{bmatrix}$$

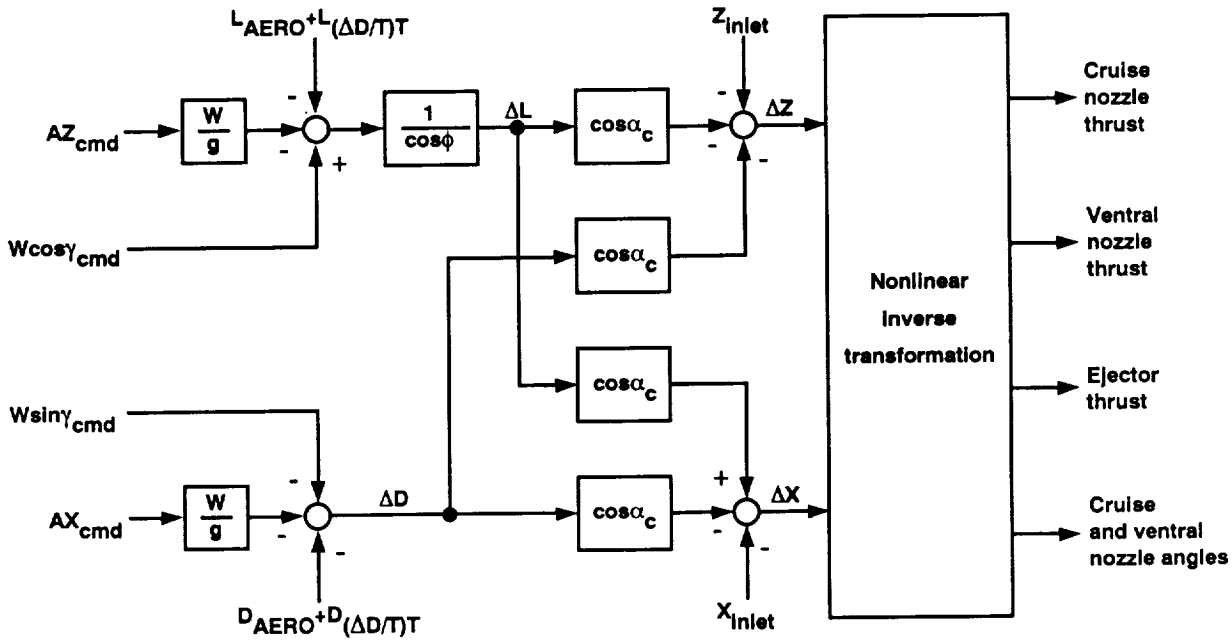

Figure 20. Thrust management system (TMS).

The 2-DCD nozzle thrust command, T_{2DC}, and nozzle angle deflection command, θ_{2DC}, are calculated from X_{2DC} and Z_{2DC}.

$$T_{2DC} = (X_{2DC}^2 + Z_{2DC}^2)^{1/2}$$

$$\theta_{2DC} = \sin^{-1}(Z_{2DC}/T_{2DC})$$

Transition– When the pitch trim demands more than available 2-DCD nozzle deflection, ventral thrust command is added to solve the longitudinal control equations. The inverse transformation equation becomes:

$$\begin{bmatrix} T_{2DC} \\ T_{VNC} \\ T_{EJC} \end{bmatrix} = \begin{bmatrix} \cos\theta_{2DC} & \cos\theta_{VNC} & 0 \\ -\sin\theta_{2DC} & -\sin\theta_{VNC} & -1 \\ D_{2DZ} & D_{VNZ} & |d_{xej}| \end{bmatrix}^{-1} \begin{bmatrix} \Delta X \\ \Delta Z \\ \Delta M \end{bmatrix}$$

In this case, 2-DCD nozzle angle command, θ_{2DC}, is fixed at its maximum downward deflection and ventral nozzle angle command, θ_{VNC}, is fixed at its maximum aft deflection.

Low speed tansition and hover– In low speed flight, the propulsion thrust is the main source of lift. The pitch trim authority is shifted from 2-DCD to ventral thrust, and the axial generalized acceleration control is also shifted from 2-DCD to ventral nozzle angle. The inverse transformation equation becomes:

$$\begin{bmatrix} X_{VNC} \\ ZVNC \\ T_{EJC} \end{bmatrix} = \begin{bmatrix} 1 & 0 & 0 \\ 0 & 1 & -1 \\ |d_{zvn}| & |d_{xvn}| & |d_{xej}| \end{bmatrix}^{-1} \begin{bmatrix} \Delta X \\ \Delta Z \\ \Delta M \end{bmatrix}$$

The ventral thrust command, T_{VNC}, and ventral nozzle deflection command, θ_{VNC}, is calculated from X_{VNC} and Z_{VNC}.

$$T_{VNC} = (X_{VNC}^2 + Z_{VNC}^2)^{1/2}$$

$$\theta_{VNC} = \sin^{-1}(X_{VNC}/T_{VNC})$$

At the limit of the propulsion system operational envelope, the integrators in the axial and vertical regulator loops are frozen until the demanded thrust falls within the propulsion system performance curve.

Simulation Experiment

Simulator Facility

This experiment was conducted on the Vertical Motion Simulator (fig. 21) at NASA Ames Research Center. The simulator provides six-degree-of-freedom motion. The simulator was equipped with a three-window fighter cockpit configuration that had a field of view of about 25° in elevation and 110° in azimuth (fig. 22). An overhead optical combining glass projected the head-up display (HUD) for the pilot. The head-up display (fig. 23) provided all key flight information to the pilot. The symbology and drive laws of the head-up display were developed specifically for STOVL aircraft flight operation by NASA Ames (ref. 5).

A linear travel throttle controller with servo drive was mounted at the left hand side of the pilot seat. The servo mechanism was used to reposition the throttle when the throttle control was switched between thrust command and flight path command. An F-16 two-axis limited displacement side arm force stick was mounted at the right hand side of the pilot and limited displacement force pedals were mounted on the floor.

The frame time for the real-time digital simulation was 20 msec. The frame time for the computer generated visual system was 16 msec and required 2 frames to completely update the screen.

Evaluation Task

The task for the pilot was to make a curved decelerating approach and land vertically on a landing pad. The visual data base for this experiment was a short take-off and landing (STOL) runway with a 40- by 70-foot landing pad. The task began at an initial speed of 200 knots in cruise mode at an altitude of 1000 feet and about 5 miles from the landing pad with an intercept heading of 65° with respect to the final approach path. The pilot was instructed to switch from cruise mode to transition mode by following a sequence of events which included lowering the landing gear, opening the ejector doors, and switching to transition mode, before he captured a 3°, 0.1g nominal decelerating approach course. The pilot then followed the approach guidance by making a left turn to align with the final approach course to the runway. The nominal decelerating schedule was reduced to 0.05 g when the aircraft came within 1000 feet range of the hover point, which was located at the center of the landing pad. After capturing the hover point 43 feet above the landing surface, the pilot switched to hover mode and landed on the landing pad vertically.

Due to limited simulator time, the task was flown in calm weather conditions with no cross wind or turbulence.

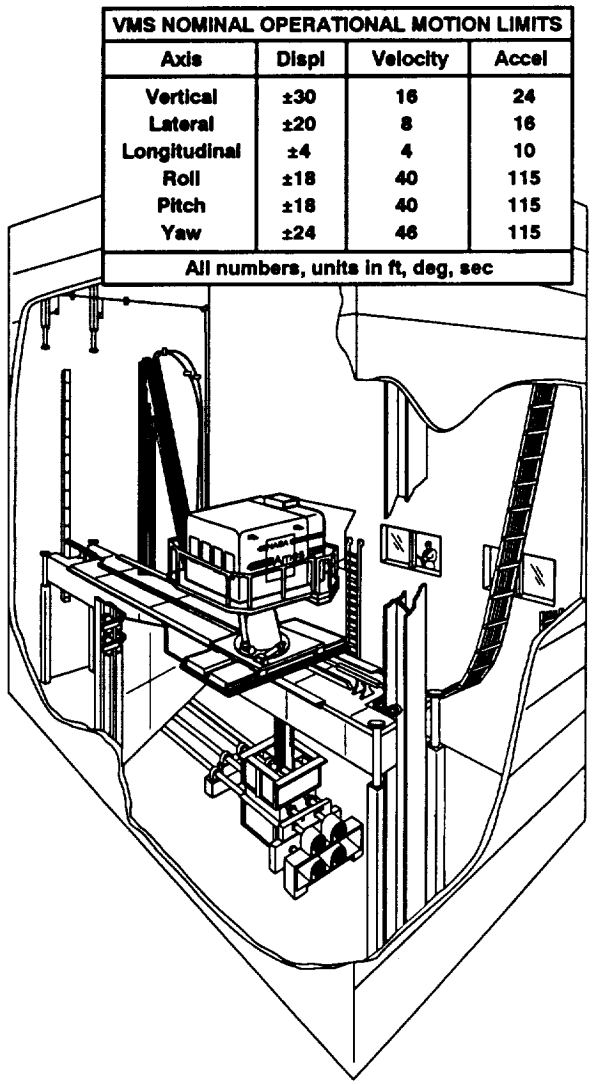

Figure 21. Vertical motion simulator.

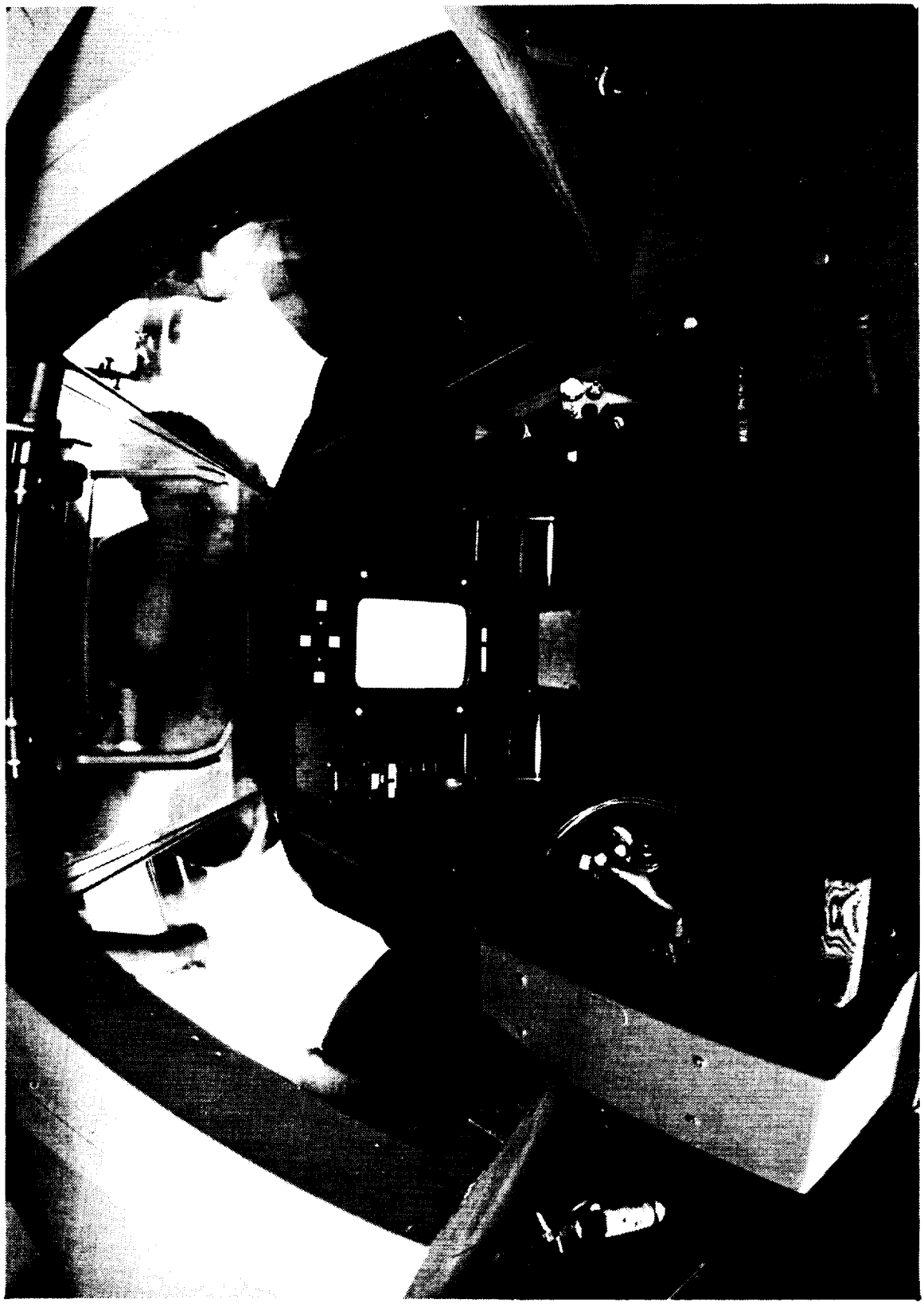

Figure 22. Simulator cockpit arrangement.

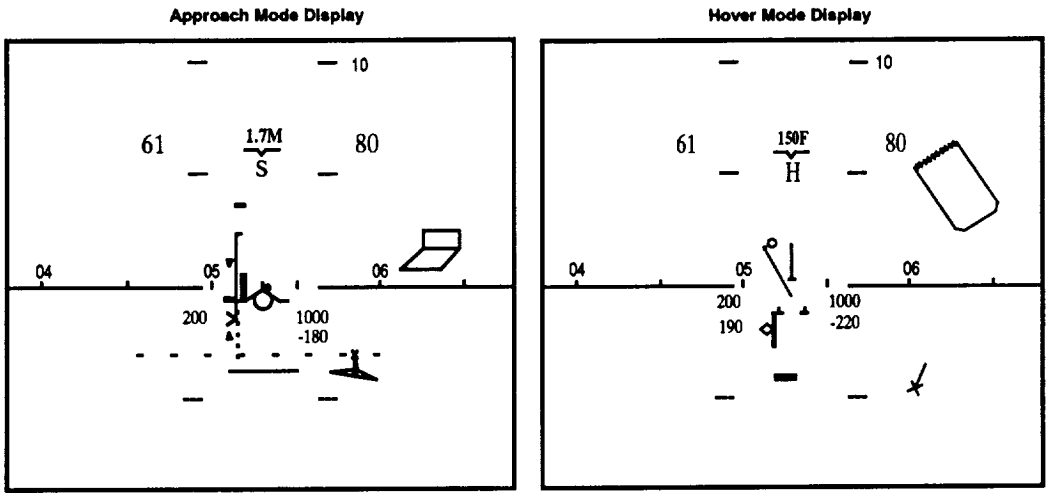

Figure 23. E7STOVL Head-up display (HUD).

Discussion of Results

Closed-Loop Response

The closed-loop response of the integrated system, except the yaw control response in hover, meets Level 1 handling qualities specifications as specified by AGARD R-577 (ref. 6) and Mil-F-83300 (ref. 7). The performance of the system is shown in table 3 in comparison with AGARD R-577 and Mil-F-83300. The frequency response of hover and transition modes are shown in figures 24–31. The bandwidth (3dB down from low frequency steady state) of each control axis is summarized as follows:

Hover– In hover, the longitudinal ground velocity command response has a bandwidth of 0.7 rad/sec. The heave axis response has a bandwidth of 1.4 rad/sec. The lateral ground velocity response has a bandwidth of 1.7 rad/sec. The yaw response has a bandwidth of 4 rad/sec.

Transition– The flight path command response has a bandwidth of 1.3 rad/sec. The pitch response has a bandwidth of 3 rad/sec. The roll rate command response has a bandwidth of 2 rad/sec. The sideslip response has a bandwidth of 0.6 rad/sec.

The closed-loop response also shows the implicit state-rate feedback model following design provides good noise rejection characteristics when subjected with disturbance (figs. 32 and 33), and zero steady state error.

Pilot Evaluation

One test pilot from NASA Ames and one test pilot from NASA Lewis flew the described task. One of the pilots also expanded the test envelope to examine the robustness of the design. Their evaluations of the handling qualities for the described task are summarized as follows:

Semi-jetborne– Control of longitudinal acceleration through the thumbwheel on the throttle was precise and de-coupled from the flight path response of the aircraft. Following the deceleration profile as presented through the deceleration error ribbon on the flight path symbol in the head-up display was effortless. Control of the flight path through the throttle lever was sufficiently responsive and likewise de-coupled from longitudinal acceleration. These control responses plus the attitude stabilization feature of the flight control system significantly reduced pilot workload and permitted a precise approach in course, glideslope and deceleration profile to the hover capture point.

Hover maneuver– Capturing the desired hover position was very easy. Once in position, the vehicle would maintain the position with no further pilot inputs required. Vertical landings required very little pilot compensation and were easily achieved.

However, during the large magnitude evaluation of the flight control system performance, there were three major deficiencies being identified by the pilots. These problems were examined and analyzed after the experiment. The problems were: Pitch departure following large acceleration or deceleration commands during hover. Uncommanded pitch oscillations during high speed transition. Lack of turn coordination on lateral-directional axes and inconsistent roll response during roll out from steady turns.

Table 3. Control power performance

Mode	Axis	Parameter	AGARD-577	Mil-83300	E7 Ames
Transition (120 Kts)	Pitch	$\ddot{\theta}_{max}$, rad/s^2	0.05–0.2		1.9
		$\theta(1)$, deg	2–4		2.5
		Control margin		50%	85%
	Roll	$\ddot{\phi}_{max}$, rad/s^2	0.1–0.6		1.6
		$\phi(1)$, deg	2–4		6.5
		$t_\phi(30°)$, sec		1–2.5	1.3
	Yaw	$\ddot{\psi}_{max}$, rad/s^2	0.15–0.25		0.58
		$t_\psi(15°)$, sec	2		1.84
		$\psi(1)$, deg		6	6.2
	Flightpath	Δa_z, g's	±0.1		±0.3
		γ, deg	6° climb–2° less than approach path angle		13° up and 10° down from level
Hover	Pitch	$\ddot{\theta}_{max}$, rad/s^2	0.1–0.3		0.3
		$\theta(1)$, deg	2–4	3	6.6
	Roll	$\ddot{\phi}_{max}$, rad/s^2	0.2–0.4		0.24
		$\phi(1)$, deg	2–4	4	3.8
	Yaw	$\ddot{\psi}_{max}$, rad/s^2	0.1–0.5		0.27
		$t_\psi(15°)$, sec	1–2.5		1.72
		$\psi(1)$, deg		6	4.9
	Heave	T/W_{min}	1.03–1.1	1.05	1.11
		$\dot{h}_{min}$, ft/min	600		1270
		Δg_{min}, g's		0.1	0.323

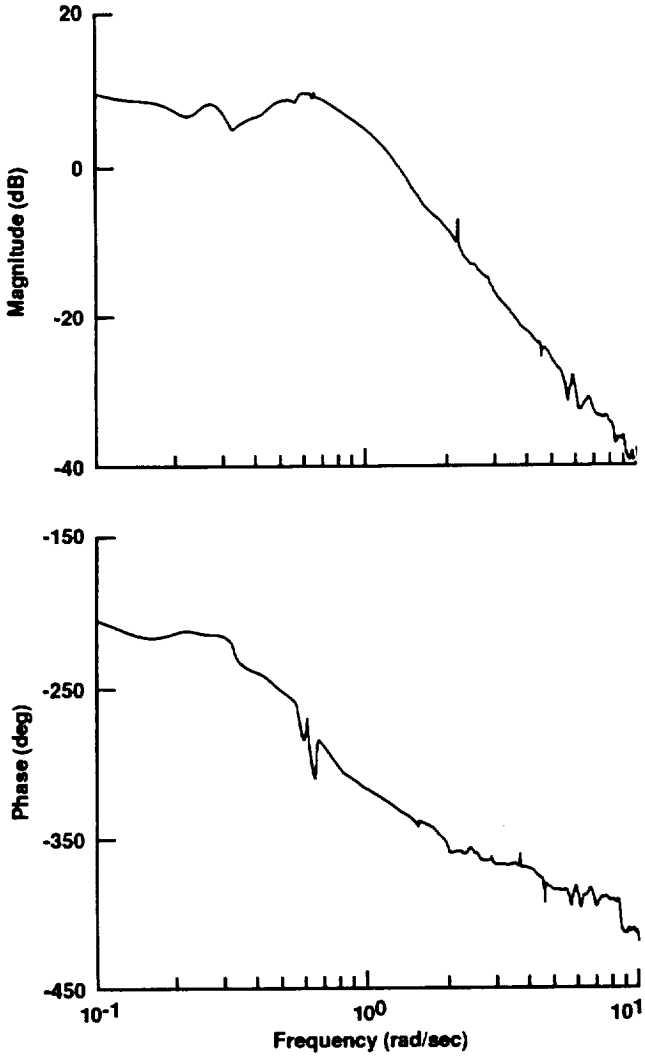

Figure 24. V_{GX}/δ_{lon} frequency response at hover.

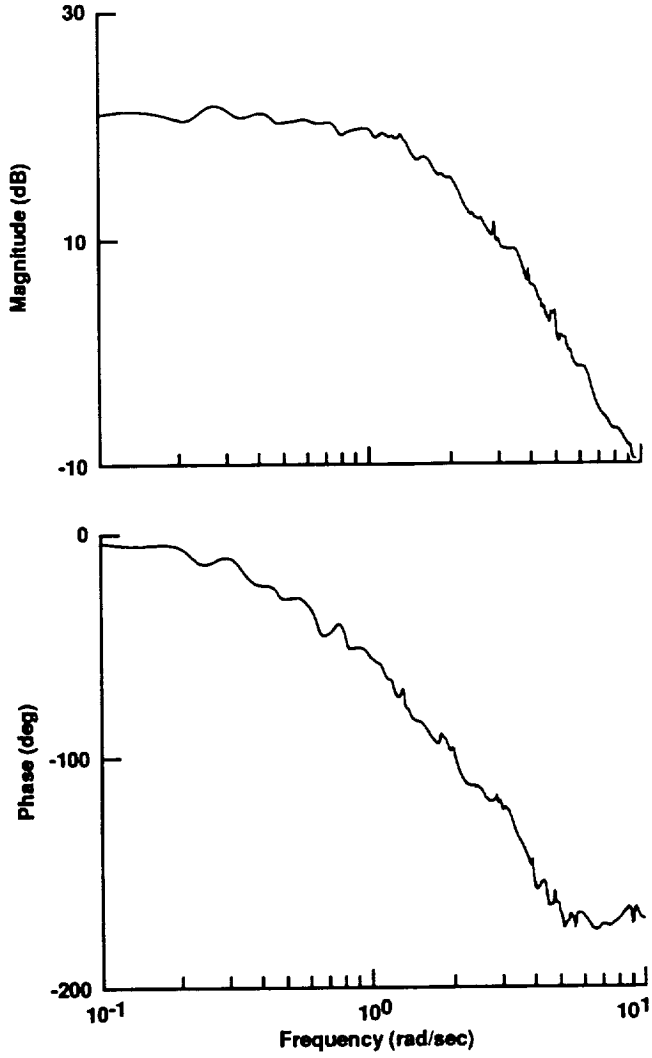

Figure 25. h/δ_{th} frequency response at hover.

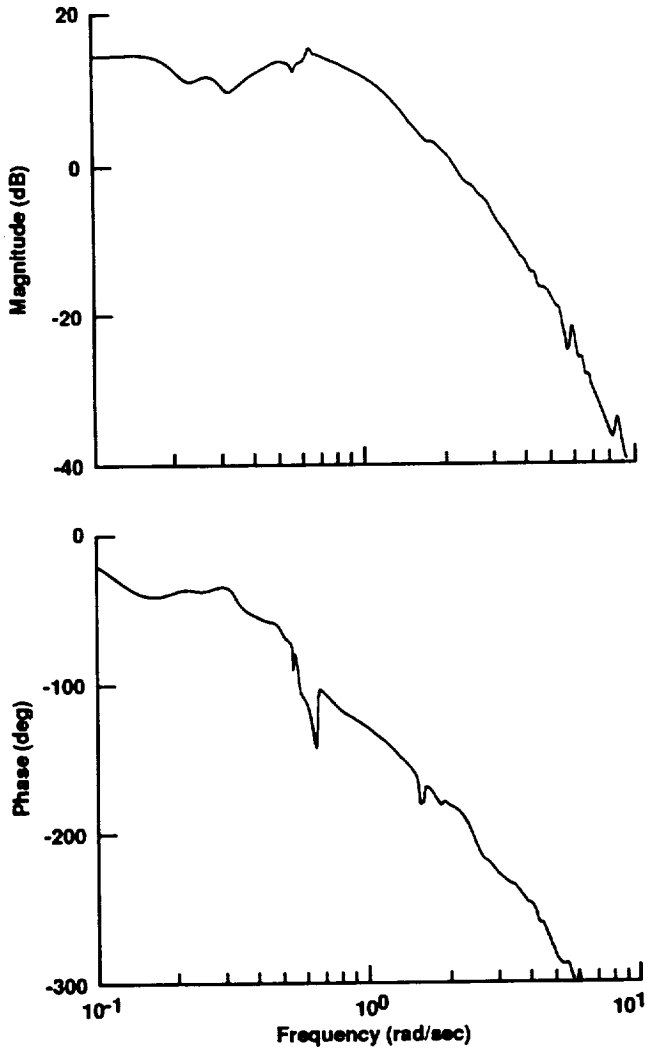

Figure 26. V_{GY}/δ_{lat} frequency response at hover.

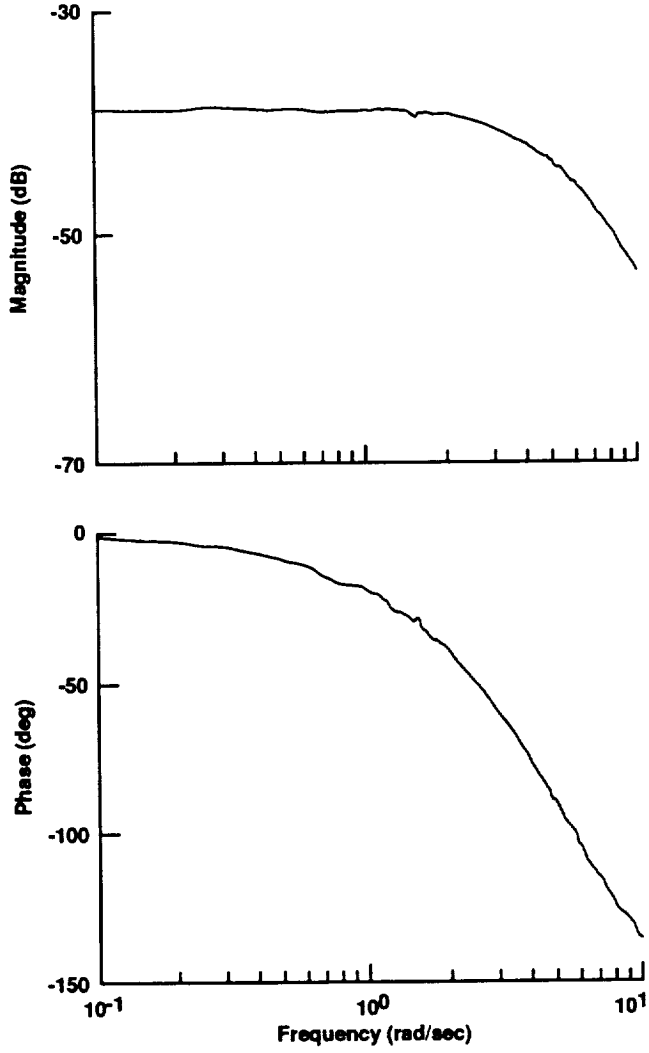

Figure 27. r/δ_{ped} frequency response at hover.

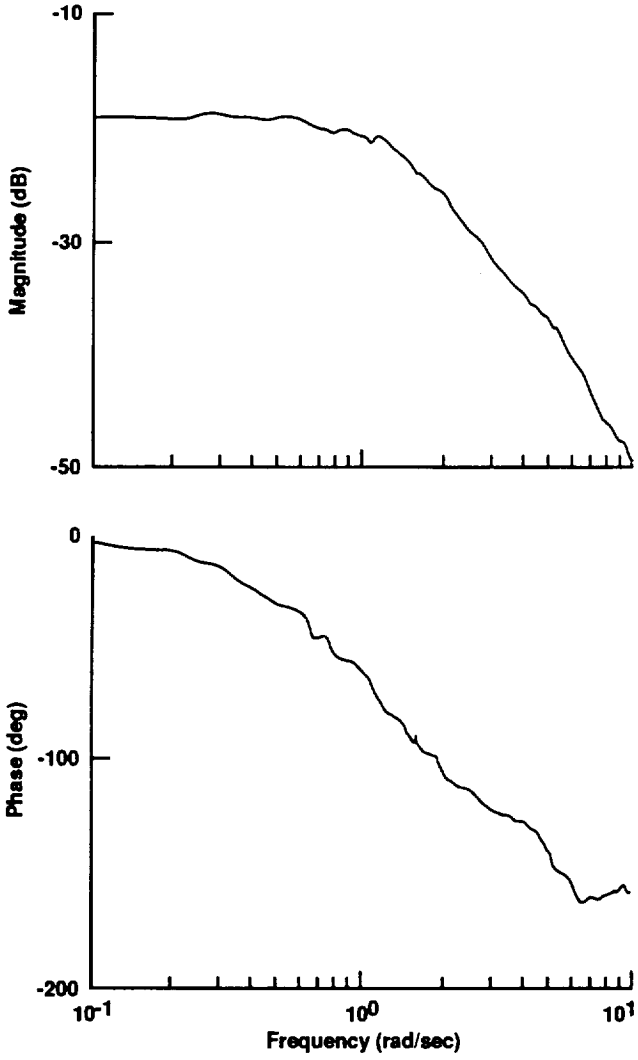

Figure 28. γ/δ_{th} frequency response at 120 knots.

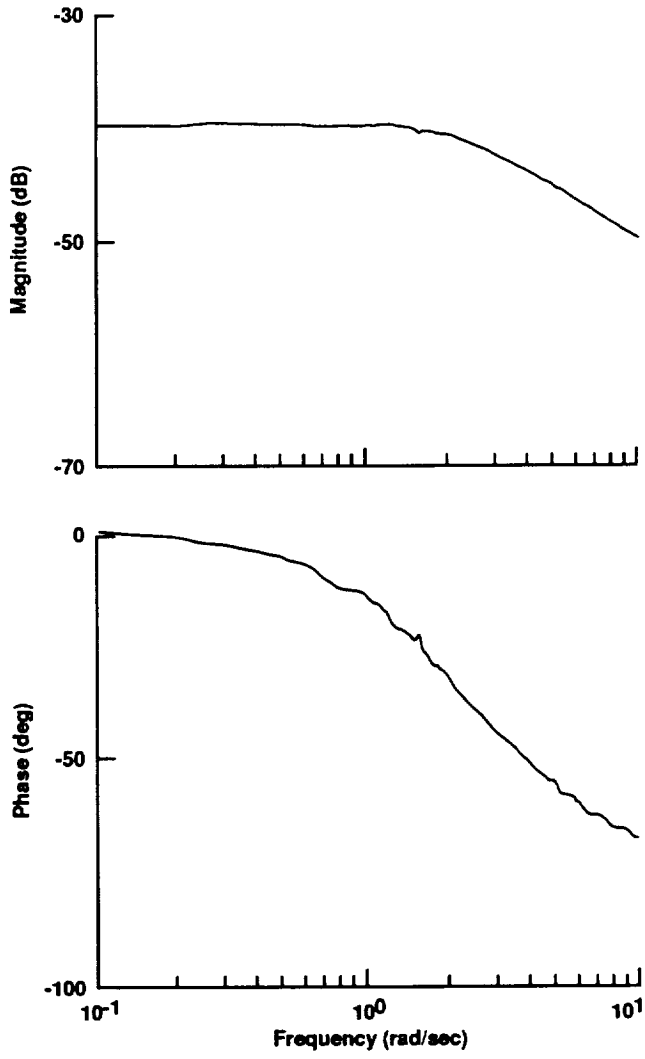

Figure 29. q/δ_{lon} frequency response at 120 knots.

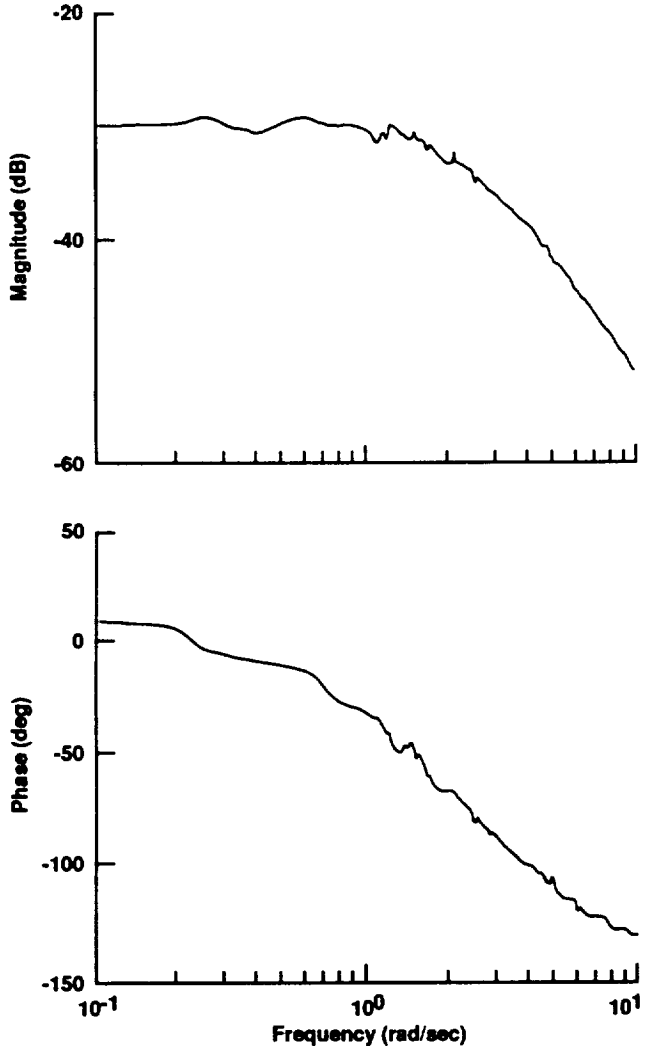

Figure 30. p/δ_{lat} frequency response at 120 knots.

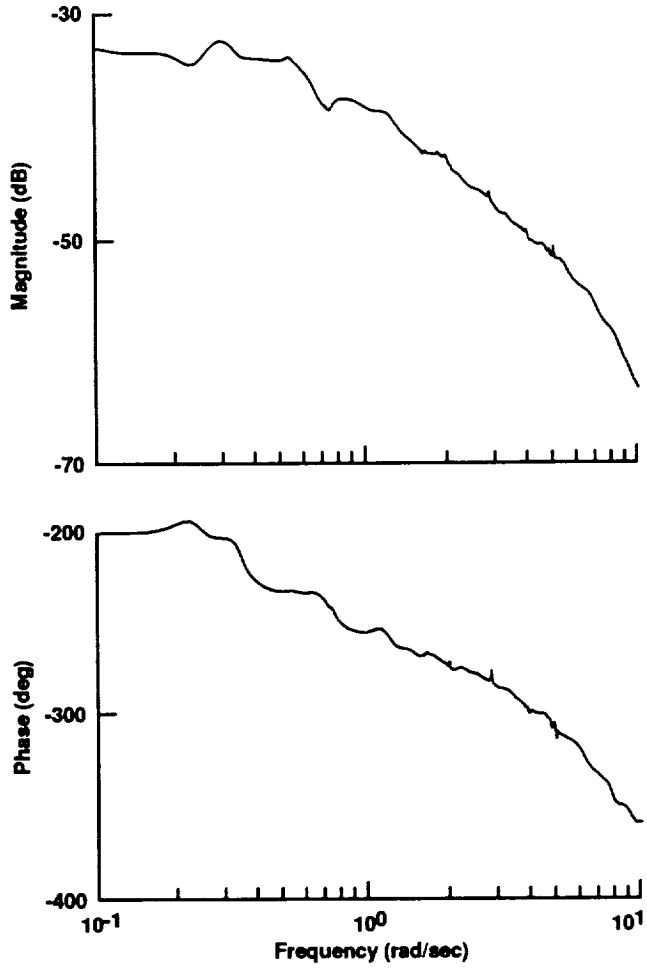

Figure 31. β/δ_{ped} frequency response at 120 knots.

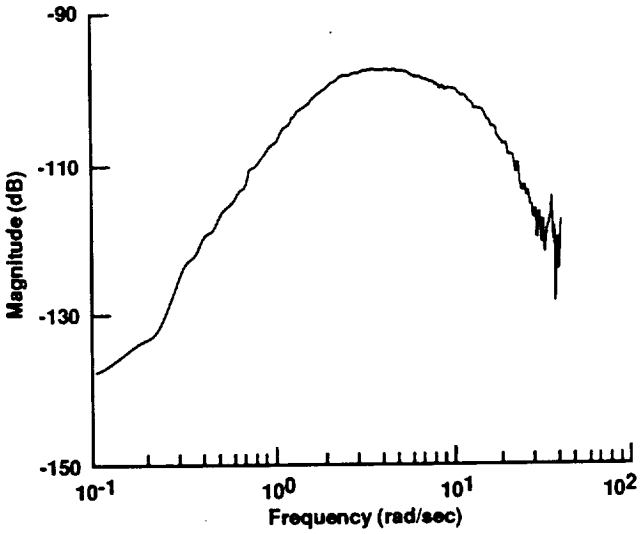

Figure 32. θ/w_{gust} (rad/ft/sec) frequency response at 75 knots.

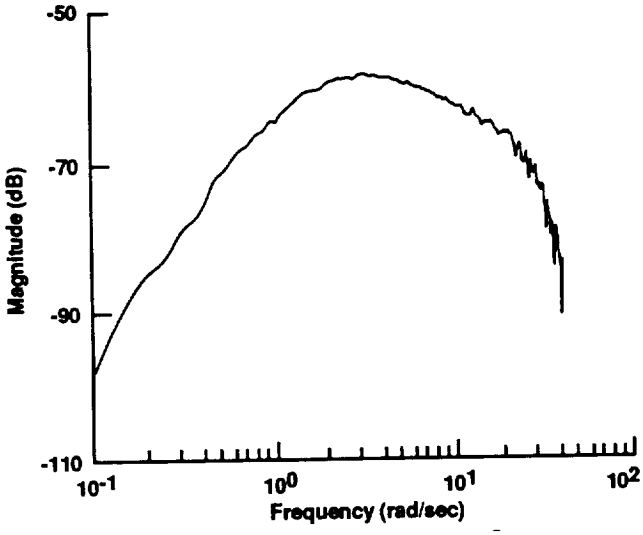

Figure 33. ϕ/v_{gust} (rad/ft/sec) frequency response at 75 knots.

The first two problems were directly related to the limiting logic in the thrust management system when the thrust commands exceeded propulsion system's maximum thrust limits. After the thrust command distribution limiting logic in the thrust management system (TMS) was modified to be in the order of priority of longitudinal acceleration, pitch trim, and vertical acceleration, the problems encountered during the simulation were corrected. Time responses of a longitudinal speed command jam in hover and a maximum acceleration in transition after the modification are shown in figures 34 and 35.

The lack of turn coordination response and inconsistent roll-out response in the lateral-directional axes were a result of poor gain schedules. After the gains were rescheduled, the turn coordination response was improved as shown in figure 36.

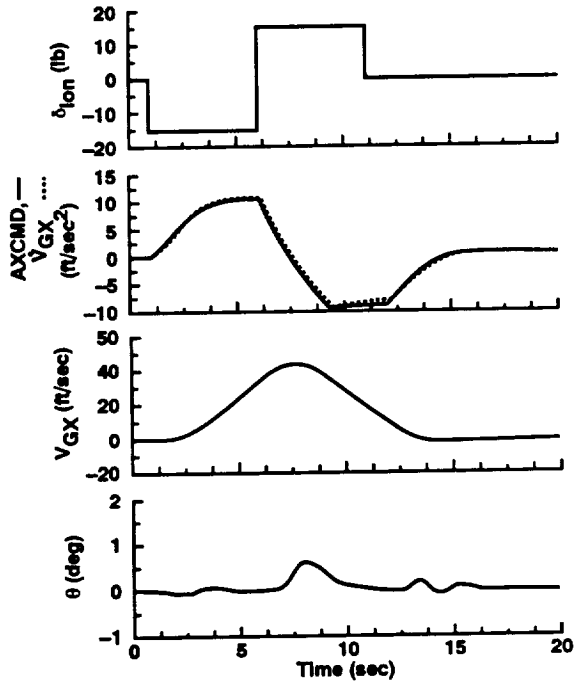

Figure 34. Maximum velocity control jam in hover.

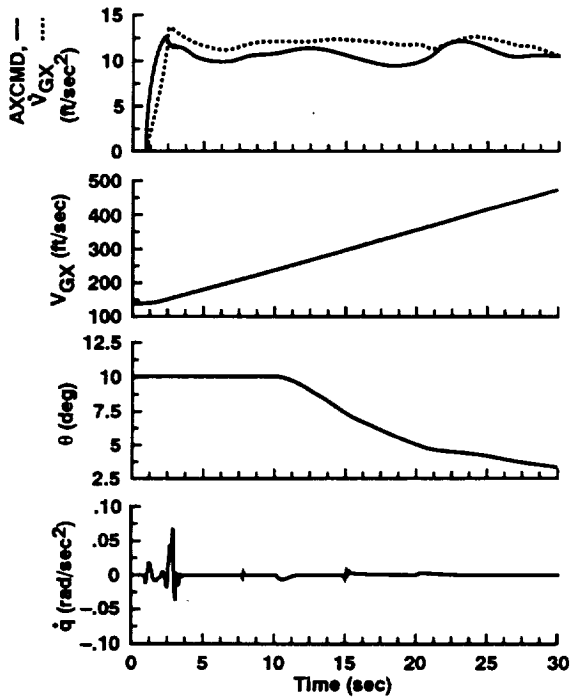

Figure 35. Maximum acceleration from 75 knots.

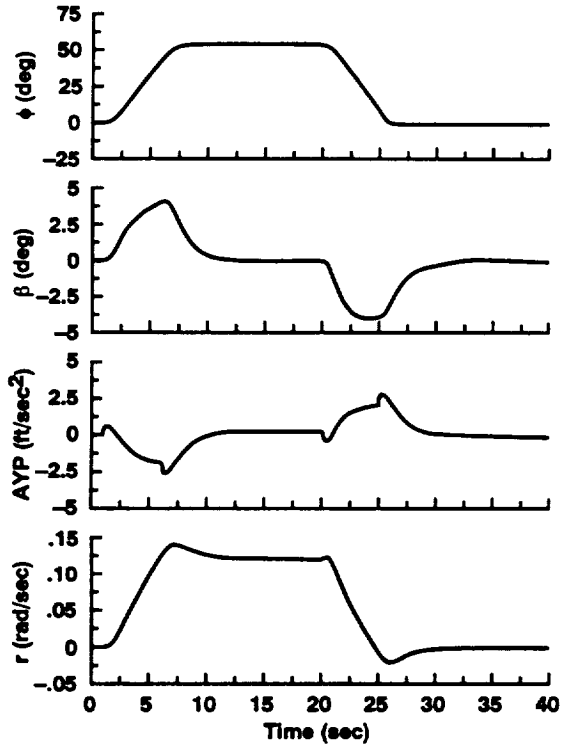

Figure 36. Turn coordination response at 120 knots.

There were two additional deficiencies being noted by the pilot regarding the throttle control effectiveness. They were:

1. Throttle was repositioned when flight control mode was switched between thrust command and flight path command. As the throttle was being repositioned, there was a period of about two to three seconds, depending on the rate of throttle servo drive, during which the pilot could not have any control over the throttle.

2. Once switched to flight path command mode, the throttle did not provide adequate flight path command authority immediately and remained ineffective until sufficient vertical thrust was developed.

Both these deficiencies are related to the flight control configuration. The flight path command augmentation requires a change on the command function of the throttle controller. That dictates the need to change the control effector's reference and sensitivity. Since the flight path command reference is chosen at the middle of the throttle travel to ensure a symmetrical flight path command authority, repositioning the throttle control becomes necessary and thus voids any pilot input during the transition.

The ejector thrust was a primary vertical acceleration contributor in the flight path command mode. However, at small butterfly valve angles, the ejector thrust response was nonlinear and oscillatory for a brief period. That response caused uncommanded pitch oscillations, which were found to be objectionable by the pilot. Realizing the limitations of the propulsion system during the experiment, two steps were taken to alleviate the problems. The ejector thrust was brought up to 1500 lb when landing gears were lowered and the flight path command was selected to be phased in when the effective thrust vector angle reached 55° and greater. That left the pilot with only flight path velocity command when he switched into the transition mode initially. The pilot was instructed to proceed to fly with the front side technique by using the pitch attitude to control vertical velocity and to follow the guidance until the flight path command was effective. This transition from frontside to backside control technique was a natural conversion in technique for a V/STOL qualified pilot and was received without objection.

Concluding Remarks

Evaluations of the non-linear inverse transformation design method on a E-7D STOVL aircraft have been conducted on a motion base simulation experiment. The objectives were to examine the implementation of the nonlinear inverse transformation method and to evaluate the handling qualities performance of the design.

The nonlinear inverse transformation method decouples the longitudinal control axes, which makes the integration of flight control system with the airframe and the propulsion system an easy and straightforward task. The TMS, which is a major part of the inverse transformation design, is developed based on the physical geometry of the propulsive nozzles' locations and deflections. Generalized control commands are distributed to individual nozzle thrust and deflection commands based on the longitudinal, vertical and pitching moment equations with known aerodynamic characteristics and thrust induced effects. Once the sequence of the propulsive pitch trim authority is determined with respect to the physical characteristics of each nozzle, the inverse transformation matrices are formed. The implicit state-rate feedback model following design provides a stable and predictable closed-loop response with good noise rejection characteristics. With the knowledge of the maximum control authorities generated from the propulsion system and the aerodynamic control surfaces, the control loop gains can be sized and tuned independently with ease.

The flight path command augmentation worked well in low speed transition. Flight path and velocity could be controlled precisely and with ease. However, this experiment showed that this flight control configuration was limited by the ejector thrust response and control inceptor configuration. The oscillatory characteristics of the ejector thrust at small butterfly valve angles warrants further improvement of the propulsion control design. During the transition from frontside technique to backside technique, the primary pilot control, i.e., throttle, was ineffective. While the pilots did not object to the change from frontside to backside technique, they did object strongly to the lack of any control through the throttle during this transition. Alternative control inceptor configuration is needed to provide effective thrust and thrust vector control for this STOVL fighter design.

References

1. Franklin, J. A.; Stortz, M. W.; Gerdes, R. M.; Hardy, G. H.; Martin, J. L.; and Engelland S. A.: Simulation Evaluation of Transition and Hover Flying Qualities of the E-7A STOVL Aircraft. NASA TM-101015, August 1988.

2. Franklin, J. A.; Stortz, M. W.; Engelland, S. A.; Hardy, G. H.; and Martin, J. L.: Moving Base Simulation Evaluation of Control System Concepts and Design Criteria for STOVL Aircraft. NASA TM-103843, June 1991.

3. Vincent, J. H.; and Anex, R.: Flight Control Design Considerations for STOVL Powered-Lift Flight. AIAA Paper 90-3225.

4. Adibhatla, S.: Propulsion Control Law Design for the NASA STOVL Control Technology Program. International Power Lift Conference, 1993.

5. Merrick, V. K.; Ferris, G. G.; and Vanags, A.A.: A Head-Up Display Format for Application to V/STOVL Approach and Landing. NASA TM-102216, September 1989.

6. Anon.: V/STOVL Handling, I – Criteria and Discussion. AGARD R-577-70, December 1970.

7. Chalk, Charles R.; Key, David L.; Kroll, John, Jr.; Wasserman, Richard; and Radford, Robert C.: Background Information and User Guide for MIL-F-83300 – Military Specification-Flying Qualities of Piloted V/STOVL Aircraft. Technical Report AFFDL-TR-70-88, November 1971.

REPORT DOCUMENTATION PAGE

Form Approved
OMB No. 0704-0188

1. AGENCY USE ONLY *(Leave blank)*	2. REPORT DATE	3. REPORT TYPE AND DATES COVERED
	May 1993	Technical Memorandum

4. TITLE AND SUBTITLE

A Direct Application of the Non-Linear Inverse Transformation Flight Control System Design on a STOVL Aircraft

5. FUNDING NUMBERS

533-02-37

6. AUTHOR(S)

W. W. Chung, W. E. McNeill, and M. W. Stortz

7. PERFORMING ORGANIZATION NAME(S) AND ADDRESS(ES)

Ames Research Center
Moffett Field, CA 94035-1000

8. PERFORMING ORGANIZATION REPORT NUMBER

A-94044

9. SPONSORING/MONITORING AGENCY NAME(S) AND ADDRESS(ES)

National Aeronautics and Space Administration
Washington, DC 20546-0001

10. SPONSORING/MONITORING AGENCY REPORT NUMBER

NASA TM-108808

11. SUPPLEMENTARY NOTES

Point of Contact: W. W. Chung, Ames Research Center, MS 200-1, Moffett Field, CA 94035-1000; (415) 604-6002

12a. DISTRIBUTION/AVAILABILITY STATEMENT

Unclassified — Unlimited
Subject Category 01

12b. DISTRIBUTION CODE

13. ABSTRACT ***(Maximum 200 words)***

The non-linear inverse transformation flight control system design method is applied to the Lockheed Ft. Worth Company's E-7D short takeoff and vertical land (STOVL) supersonic fighter/attack aircraft design with a modified General Electric F110 engine which has augmented propulsive lift capability. The system is fully augmented to provide flight path control and velocity control, and rate command attitude hold for angular axes during the transition and hover operations. In cruise mode, the flight control system is configured to provide direct thrust command, rate command attitude hold for pitch and roll axes, and sideslip command with turn coordination. A control selector based on the non-linear inverse transformation method is designed specifically to be compatible with the propulsion system's physical configuration which has a two-dimensional convergent-divergent aft nozzle, a vectorable ventral nozzle and a thrust augmented ejector. The non-linear inverse transformation is used to determine the propulsive forces and nozzle deflections, which in combination with the aerodynamic forces and moments (including propulsive induced contributions), and gravitational force, are required to achieve the longitudinal and vertical acceleration commands. The longitudinal control axes are fully decoupled within the propulsion system's performance envelope. A piloted motion-base flight simulation was conducted on the Vertical Motion Simulator (VMS) at NASA Ames Research Center to examine the handling qualitites of this design. Based on results of the simulation, refinements to the control system have been made and will also be covered in the report.

14. SUBJECT TERMS	15. NUMBER OF PAGES
STOVL, Non-linear inverse transformation, Flight control systems	28
	16. PRICE CODE: A03

17. SECURITY CLASSIFICATION OF REPORT	18. SECURITY CLASSIFICATION OF THIS PAGE	19. SECURITY CLASSIFICATION OF ABSTRACT	20. LIMITATION OF ABSTRACT
Unclassified	Unclassified		